NAVAL POSTGRADUATE SCHOOL
Monterey, California

THESIS

DETERMINATION OF INCLUSION CHEMISTRY AND SIZE DISTRIBUTION IN STEEL WELDMENTS BY ANALYTICAL ELECTRON MICROSCOPY

by

Craig Allen Hackstaff

June 2001

Thesis Advisor: Alan G. Fox

Approved for public release; distribution is unlimited.

REPORT DOCUMENTATION PAGE		Form Approved OMB No. 0704-0188

Public reporting burden for this collection of information is estimated to average 1 hour per response, including the time for reviewing instruction, searching existing data sources, gathering and maintaining the data needed, and completing and reviewing the collection of information. Send comments regarding this burden estimate or any other aspect of this collection of information, including suggestions for reducing this burden, to Washington headquarters Services, Directorate for Information Operations and Reports, 1215 Jefferson Davis Highway, Suite 1204, Arlington, VA 22202-4302, and to the Office of Management and Budget, Paperwork Reduction Project (0704-0188) Washington DC 20503.

1. AGENCY USE ONLY *(Leave blank)*	2. REPORT DATE June 2001	3. REPORT TYPE AND DATES COVERED Master's Thesis

4. TITLE AND SUBTITLE: Title (Mix case letters)
Determination of Inclusion Chemistry and Size Distribution in Steel Weldments by Analytical Electron Microscopy

5. FUNDING NUMBERS

6. AUTHOR(S)
Hackstaff, Craig A.

7. PERFORMING ORGANIZATION NAME(S) AND ADDRESS(ES)
Naval Postgraduate School
Monterey, CA 93943-5000

8. PERFORMING ORGANIZATION REPORT NUMBER

9. SPONSORING / MONITORING AGENCY NAME(S) AND ADDRESS(ES)
Naval Surface Warfare Center, Carderock Division

10. SPONSORING / MONITORING AGENCY REPORT NUMBER

11. SUPPLEMENTARY NOTES The views expressed in this thesis are those of the author and do not reflect the official policy or position of the Department of Defense or the U.S. Government.

12a. DISTRIBUTION / AVAILABILITY STATEMENT
Approved for public release; distribution is unlimited

12b. DISTRIBUTION CODE

13. ABSTRACT ***(maximum 200 words)***

The U. S. Navy has been concerned about reducing the number of inclusions in steel weldments to increase the toughness of the weld metal. Research has shown that particular inclusions can nucleate the acicular ferrite microstructure in the weld metal, which can increase toughness without compromising strength. The present study investigated the inclusion chemistry and size distribution in aluminum-deoxidized C-Mn steel weldments. The results showed that the addition of aluminum to the C-Mn weld metal will produce inclusions, that can nucleate acicular ferrite by epitaxy, and that the number and volume fraction of inclusions is reduced. This indicates that aluminum deoxidation of steel weld metal can have positive benefits for C-Mn weld metal strength and toughness.

14. SUBJECT TERMS Acicular Ferrite, Shielded Metal Arc Welding, C-Mn Steel Weldments, Non-metallic Inclusions			15. NUMBER OF PAGES 100 16. PRICE CODE
17. SECURITY CLASSIFICATION OF REPORT Unclassified	18. SECURITY CLASSIFICATION OF THIS PAGE Unclassified	19. SECURITY CLASSIFICATION OF ABSTRACT Unclassified	20. LIMITATION OF ABSTRACT UL

NSN 7540-01-280-5500

Standard Form 298 (Rev. 2-89)
Prescribed by ANSI Std. 239-18

THIS PAGE INTENTIONALLY LEFT BLANK

Approved for public release; distribution is unlimited.

DETERMINATION OF INCLUSION CHEMISTRY AND SIZE DISTRIBUTION IN STEEL WELDMENTS BY ANALYTICAL ELECTRON MICROSCOPY

Craig A. Hackstaff
Lieutenant, United States Navy
B.S., United States Naval Academy, 1994

Submitted in partial fulfillment of the
requirements for the degree of

MASTER OF SCIENCE IN MECHANICAL ENGINEERING

from the

NAVAL POSTGRADUATE SCHOOL
June 2001

Author: _____
Craig A. Hackstaff

Approved by: A. G. Fox
Alan G. Fox, Thesis Advisor

_____
Terry R. McNelley, Chairman
Department of Mechanical Engineering

THIS PAGE INTENTIONALLY LEFT BLANK

ABSTRACT

The U. S. Navy has been concerned about reducing the number of inclusions in steel weldments to increase the toughness of the weld metal. Research has shown that particular inclusions can nucleate the acicular ferrite microstructure in the weld metal, which can increase toughness without compromising strength. The present study investigated the inclusion chemistry and size distribution in aluminum-deoxidized C-Mn steel weldments. The results showed that the addition of aluminum to the C-Mn weld metal will produce inclusions, that can nucleate acicular ferrite by epitaxy, and that the number and volume fraction of inclusions is reduced. This indicates that aluminum deoxidation of steel weld metal can have positive benefits for C-Mn weld metal strength and toughness.

THIS PAGE INTENTIONALLY LEFT BLANK

TABLE OF CONTENTS

THIS PAGE INTENTIONALLY LEFT BLANK

LIST OF FIGURES

THIS PAGE INTENTIONALLY LEFT BLANK

LIST OF TABLES

THIS PAGE INTENTIONALLY LEFT BLANK

ACKNOWLEDGMENTS

I would like to express my appreciation and gratitude to Dr. Alan G. Fox for his guidance, humor, and enthusiasm during the process of this thesis.

I would also like to extend a special acknowledgement to Mr. Chan Park for his assistance in the laboratory.

Finally, I would like to thank my mother, Susan, brother, Andrew, and grandmother, Helen, for their love and support. And to Robin, I love and thank you for being by my side.

THIS PAGE INTENTIONALLY LEFT BLANK

I. INTRODUCTION

Since the beginning of human existence, man has acquired materials and formed them into useful tools. In fact, ancient civilizations were named after man's mastery of materials during the period concerned, e.g. Iron Age. Materials were perhaps the greatest discovery of ancient civilizations, who learned how to produce and manipulate them for tools and structures. Today, steel has been incorporated into almost every type of structure, such as bridges, buildings and ships. With steel having excellent qualities, such as strength, it has become the most studied in its manufacturing, processing and performance. In the first half of the 20^{th} century, the joining of steel changed from rivets and bolts to welding. Even though high quality steels have been developed, the poor toughness of the welded joint often has detrimental effects on finished structures.

In order to achieve weld metal strength and toughness that is similar to the base plate, the welding process must be carefully controlled. In ferritic steel welding, a weld microstructure containing considerable amounts of acicular ferrite has been discovered to yield qualities similar or even superior to that of the base plate. The complexity of acicular ferrite nucleation makes it critically important to understand and control.

Most arc welding methods can produce acicular ferrite in the weld metal. The most common types of arc welding used today are Shielded Metal Arc (SMAW), Gas Metal Arc (GMAW), Gas Tungsten Arc (GTAW), and Submerged Arc (SAW). Common microstructural constituents in ferritic steel welds include: bainite,

martensite, grain boundary ferrite, side plate ferrite, and acicular ferrite. Acicular ferrite is the only microstructural constituent that improves the strength and toughness of the weld metal, providing that it is present in significant amounts, and this is possible for SMAW, GMAW, and SAW. Acicular ferrite is less likely in ferritic steel weld metals deposited by GTAW because it is a very "clean" welding process.

Through optical microscopy, it has been found that acicular ferrite nucleates intragranularly on small nonmetallic inclusions, producing an almost woven-like microstructure. This woven-like microstructure is extremely resistant to crack propagation. Reducing the amount and size of inclusions also increases the strength and toughness of the weld metal since inclusions are potential crack initiation sites. Utilization of the proper alloying elements that both promote the formation of acicular ferrite and reduce the number and size of inclusions is extremely important. The relationship between the nonmetallic inclusions and acicular ferrite nucleation is still not understood due to the complexity of the reaction at the interface between the inclusions and the steel matrix.

The intention of the present work is to provide a better understanding of the relationship between nonmetallic inclusions and the mechanism of acicular ferrite nucleation by using Scanning Electron Microscopy (SEM) and Transmission Electron Microscopy (TEM). This information will aid in the development of core wires, flux and filler wires for ferritic steel welding.

II. BACKGROUND

A. SHIELDED METAL ARC WELDING

Shielded metal arc welding (SMAW) is an arc welding process that uses an electric arc to heat and melt a covered consumable electrode to the base metal. A sketch of the SMAW process is shown in Figure 2-1. The electrode usually contains various filler metal and layered fluxes. The flux covering can contain various chemicals and even metals. For steel welding, fluxes with little or no hydrogen are used to prevent hydrogen embrittlement within the weld. Also, the flux covering can be baked so that all excess moisture and hydrogen are removed. The electrode can perform one or more of the following functions [Ref. 1]:

- Provide a gaseous shield to protect the weld pool from the environment.
- Provide deoxidizers to deoxidize and clean the weld pool.
- Provide arc stabilizers to maintain a stable arc during the process.
- Provide alloying elements to the weld.

SMAW is often used for maintenance, repair and construction. Compared to other arc welding processes, SMAW equipment is relatively inexpensive, portable, and simple.

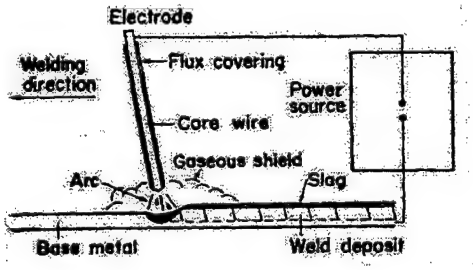

Figure 2-1. Sketch of the SMAW process from [Ref. 1].

B. WELD METAL

1. General Microstructure

A typical single weld pass can be divided into three distinct regions: the fusion zone (FZ), the heat affected zone (HAZ), and the base metal. Inside the HAZ, the partial grain coarsening region is located near FZ, the grain refining zone is near the center of the HAZ, and the partial grain refining zone is region near the interface with the base metal. A sketch of a typical single pass, ferritic steel weld with the various regions is shown in Figure 2-2 [Ref. 1].

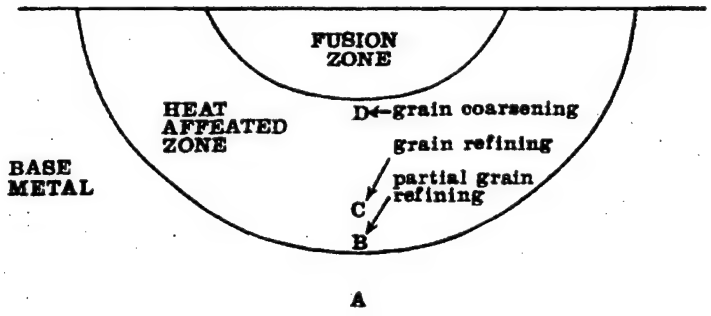

Figure 2-2. A sketch of a typical single pass, steel weld from [Ref. 1].

The liquefied weld pool solidifies to form the fusion zone. The grain structure is determined by epitaxial and competitive growth, the weld pool composition, and the welding parameters. Generally, the grains grow from the substrate, the unmelted base metal, toward the center of the weld, resulting in long columnar grains. The long grains form due to the high heat input supplied by the electric arc. During solidification, the maximum thermal gradient is perpendicular to the solid/liquid interface. As a result, if sulfur and carbon contents are high, solidification cracking may occur [Ref. 1].

A sketch of the typical fusion zone microstructure is shown below in Figure 2-3.

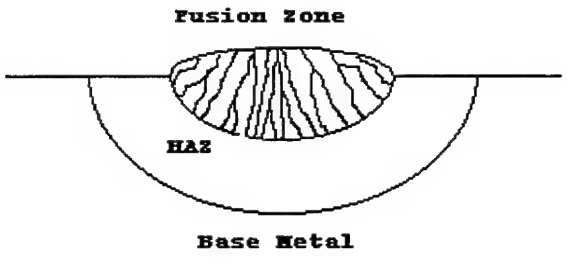

Figure 2-3. Sketch of the typical fusion zone microstructure.

The Heat Affected Zone (HAZ) is the most complex zone within the weld. The main reason the HAZ is complex is that it experiences a wide temperature difference between the molten fusion zone and the base metal. With multiple weld passes, the temperature gradients experienced result in complex microstructures for which there are numerous continuous cooling transformation (CCT) diagrams too complex to even generate. [Ref. 2].

The grain-coarsening zone of the HAZ experiences the highest temperatures. The resulting microstructure is large grains and these grains are relatively smaller than those in the fusion zone. The grain-coarsening region may experience rapid cooling rates, which may lead to the formation of bainite and martensite. These particular microstructures are detrimental to the toughness of the HAZ, since bainite and martensite can be brittle particularly if they exist in an untempered state.

The grain refining region of the HAZ experiences temperatures that promote austenite grain nucleation but they are low enough that significant coarsening does not occur. The subsequent microstructure is very fine grains of pearlite and ferrite for C-Mn steels for most heat inputs. These microstructures are not evenly distributed due to the insufficient time for the carbon to diffuse from the austenite grains. This region is the toughest in the HAZ.

The partial grain refining region experiences temperatures that are lower than the other regions. Some reaustenitization of the pearlite colonies occurs, but the prior ferrite colonies remain unchanged. Fine grains of pearlite and ferrite form upon cooling.

2. Weld Metal Microconstituents

A final steel weld metal microstructure is extremely complex, especially if multiple passes are used. The final microstructure is determined by the cooling rate, alloying elements, heat input, and the oxygen content [Ref. 1]. A schematic continuous cooling transformation diagram is shown in Figure 2.4. The figure shows how any changes in the aforementioned weld characteristics would influence the microstructure and ultimately influence the mechanical properties of the weld.

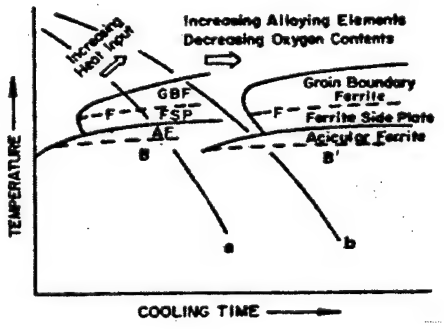

Figure 2-4. CCT diagram for the weld of low carbon, low alloy steel from [Ref. 1].

Due to the variety of nomenclatures for the microstructural constituents, the International Welding Society established guidelines for the optical classification of the major constituents found in steel weld metals [Ref. 3]. These guidelines define the following weld microstructures:

a. Primary Ferrite (PF)

Primary ferrite is the first microstructural constituent that forms from cooling of the prior austenite. Grain boundary ferrite and intragranular polygonal ferrite are the two possible forms of primary ferrite. Grain boundary ferrite, also known as allotriomorphic ferrite, transforms at the prior austenite grain boundaries. Intragranular ferrite forms within the austenite grain boundaries. Primary ferrite is a diffusion controlled reaction at high temperatures and slow cooling rates. Primary ferrite is much larger than acicular ferrite and ferrite with second phase.

b. Ferrite Carbide Aggregate (FC)

Ferrite carbide aggregate consists of ferrite with interphase carbides, which form at high temperatures with long cooling rates. A primary example of this is pearlite, consisting of lamellae of ferrite and cementite. The lamellae or layers of cementite and ferrite transform from austenite to form simultaneously due to diffusion of carbon [Ref. 4]. This type of microstructure is rarely seen in ferritic steel weld metals because most welding processes have fast cooling rates.

c. Ferrite with Second Phase (FS)

Due to the fine microstructure from fast cooling rates in welds, the individual microstructural constituents are extremely difficult to observe using optical microscopy since its limit of spatial resolution is poor. For this reason, the certain

microstructural constituents are grouped into ferrite with second phase. The ferrite with second phase constituent contains both aligned second phase and non-aligned second phase. Aligned second phases include Widmanstätten, also known as side-plate, ferrite, upper and lower bainite, and tempered martensite. Compared to primary ferrite, side-plate ferrite forms at lower temperatures and at faster cooling rates. Side-plate ferrite nucleates perpendicular to the ferrite-austenite grain boundary, using a displacive mechanism at the grain boundary [Ref. 4]. Bainite is a needle-like microstructure containing ferrite laths with cementite in between the laths. Bainite forms at lower temperatures compared to side-plate ferrite. Upper bainite forms at higher temperatures while lower bainite forms at lower temperatures, producing a finer microstructure [Ref. 5]. Tempered martensite is a fine needle-like microstructure, which is extremely hard and brittle. It forms at very fast cooling rates. Ferrite with non-aligned second phase is mainly associated with the microstructures surrounding the laths of acicular ferrite.

d. Acicular Ferrite (AF)

Acicular ferrite is the most desirable microstructural constituent because it is very effective in stopping crack propagation. Acicular ferrite increases the toughness and strength of the weld metal. Acicular ferrite forms intragranularly but nucleates on non-metallic inclusions, unlike bainite, which forms on the grain boundaries. Figure 2-5 is a diagram illustrating the difference between bainite and acicular ferrite. Acicular ferrite forms a basket-weave microstructure by ferrite plates (which appear as needles in two dimensional sections) radiating from the inclusions, by a displacive-diffusion process [Ref. 6, 7, 8]. The basket-weave microstructure and small plate size both contribute to the strength and toughness. Acicular ferrite forms at cooling rates similar to those required

for bainite formation. It should be noted that a large (~80 μm width) austenite grain size such as hat found in steel weld metals is necessary for acicular ferrite formation. This is shown schematically in Figure 2-5.

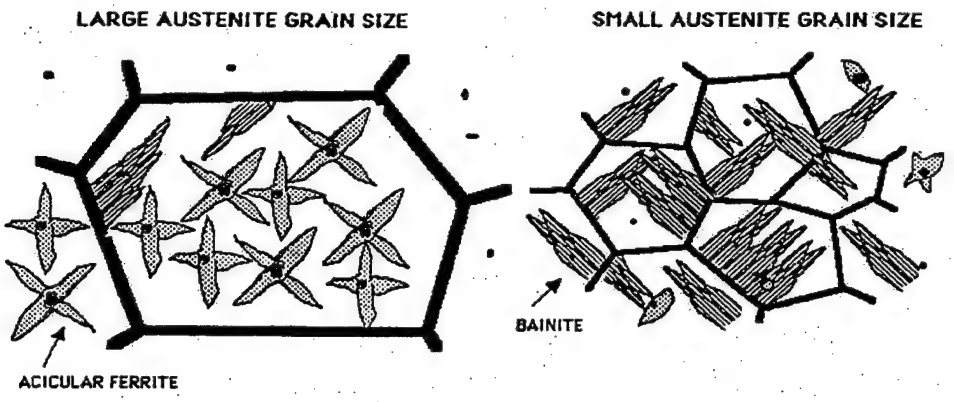

Figure 2-5. Sketch of the difference between acicular ferrite and bainite from [Ref. 4].

3. Multipass Effects

The determination of mechanical properties for multi-pass welds is extremely complex due to thermal history, chemical composition, and microstructural properties. The microstructure and thus mechanical properties of a single weld deposit can be readily assessed. However, for multi-pass welds, subsequent weld passes affect each previous one and thus make such an assessment more difficult. Figure 2-6a. is a schematic diagram of a multi-pass weld and 2-6b. is an actual picture of a multi-pass weld. If the interpass temperature rises high enough, the previous weld can reaustenitize and then, cool to a different microstructure than it was previously. Some previous welds may temper and their mechanical properties will thus be changed. This is dependent on the previous microstructure and alloy chemistry [Ref. 9]. Generally, the final microstructure cannot be easily predicted. Modeling and experimental work have tried to evaluate the

effects of thermal cycling on the weld toughness, however, little ground has been made to effectively predict the mechanical properties. Poor mechanical properties can be associated with large grains that have not been reaustenitized particularly if they contain untempered martensite.

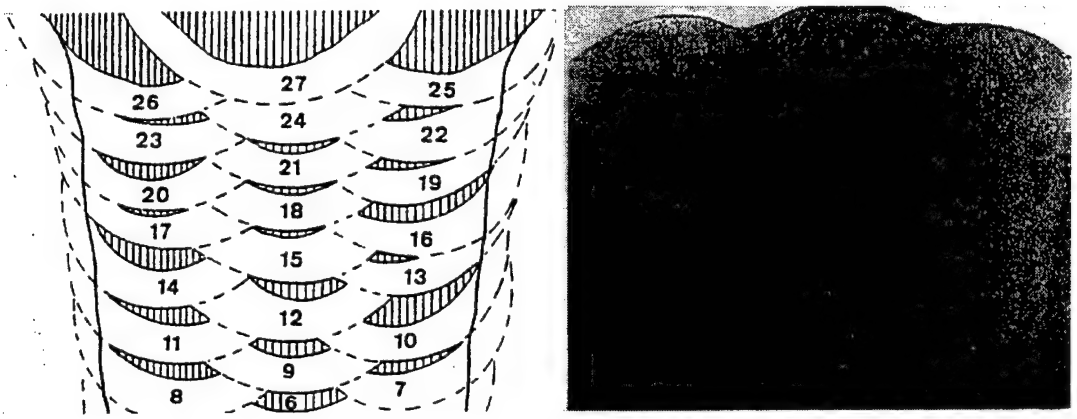

a. b.

Figure 2-6. a. Schematic of a 27-run weld from [Ref. 10]. b. Actual multi-pass weld

C. NON-METALLIC INCLUSIONS

1. General

The production of steel and steel weld metals always generates impurities in the form of non-metallic inclusions, which can either be beneficial or detrimental to weld toughness, depending on their characteristics. These characteristics include chemistry, size distribution, and morphology. These inclusions exist as sulfides, nitrides, and oxides. Oxygen, sulfur, and nitrogen interact with the alloying elements in the weld pool, which are provided by the base metal and the flux. Indigenous inclusions are inclusions that form from homogenous reaction with the sulfur, nitrogen, and oxygen. Exogenous inclusions are formed from impurities and slag that have not escaped the molten weld

pool. Exogenous inclusions are almost always detrimental to the toughness of welds. In fact, all inclusions in steel weld metal are detrimental to toughness unless they are very small (~ 0.1 μm or less) and constrain grain size or are somewhat larger (~0.5 μm) and are effective at nucleating acicular ferrite [Ref. 11]. Larger inclusions usually lead to crack initiation sites and can cause premature failure of the weld metal.

2. Deoxidation

As a general rule, lowering the amount of dissolved and undissolved (inclusion) oxygen in a weld improves the toughness of the weld upon solidification. The filler wire and fluxing agents add deoxidizing elements such as aluminum, titanium, manganese, and silicon into the weld. These deoxidizers react with the oxygen and form non-metallic inclusions. Without deoxidizers, compounds such as FeO can cause brittle failure. Figure 2-7 is a diagram of the free energies of the formation of various oxides. As shown in Figure 2-7, the free energy of formation for the alloying elements is considerably lower than the formation of FeO. This means that these other oxides are more likely to form than FeO. Another result of deoxidizing the weld is the possible formation of carbon monoxide (when deoxidant levels are low). This can cause porosity and thus crack initiation sites [Ref. 1]. Common deoxidizers are discussed below.

a. Aluminum

Between aluminum, titanium, silicon, and manganese, aluminum is the strongest deoxidant, with the lowest free energy in Figure 2-7. Alumina, Al_2O_3, is the product of the reaction between aluminum and oxygen. Alumina is often found in

considerable concentrations in inclusions if significant quantities of aluminum are present in the weld. Previous work has shown that γ-alumina is effective at nucleating acicular ferrite [Ref. 12, 13, 14]. γ-Alumina has a high melting point, and since cooling rates are rapid in welding, δ- and α-alumina may not form. γ-Alumina has a cubic microstructure, which has been shown to nucleate acicular ferrite through epitaxy [Ref. 15]. This will be discussed later in the next major section.

b. Titanium

According to Figure 2-7, titanium has the second lowest free energy of formation, which makes it the second strongest deoxidant. There are numerous ways in which oxygen can react with titanium. The different titanium oxide formations include TiO, TiO_2, and Ti_2O_3 [Ref. 13, 16, 17]. In addition, complex oxides such as $MnO.TiO_2$ and $MnO.Ti_2O_3$ have been reported. However, there is much controversy as to which form of titanium oxide most effectively promotes acicular ferrite and why it does so. In addition, TiN has been found to promote acicular ferrite by epitaxy when the dissolved oxygen content is low due to its removal by Al_2O_3 [Ref. 15]. It has been suggested that titanium oxide can be very effective at nucleating acicular ferrite through chemical reaction [Ref. 18, 19], and this will be discussed later in the next major section.

c. Silicon

Silicon is the third strongest deoxidant although it is a relatively weak deoxidizer. Silicon reacts with oxygen to form silica, SiO_2 and also more complex oxides such as $MnO.SiO_2$. Silica has been shown to be an effective, but not a strong acicular ferrite nucleator [Ref. 20]. Large amounts of silicon, greater than approximately 0.5 wt%, can be detrimental to the toughness of the weld [Ref. 21].

d. Manganese

Manganese is the weakest of the four alloying elements that usually deoxidize the weld metal. Manganese reacts with oxygen to form MnO and other complex oxides, such as $MnO.SiO_2$ and $MnO.Al_2O_3$. Abson and Pargeter indicate that manganese oxide-based inclusions can nucleate acicular ferrite [Ref. 21]. For the cubic phase $MnO.Al_2O_3$ (galaxite), Grong et al. [Ref. 15] have shown that acicular ferrite can be nucleated by epitaxy. The addition of manganese also promotes the formation of MnS, which reduces the chances of FeS forming. This is beneficial because MnS reduces the likelihood of solidification cracking, hence increases the toughness [Ref.1].

3. Desulfurization

Removal of sulfur in a weld is extremely important because the sulfur may react with the iron in the steel to form FeS. FeS forms a film at grain boundaries, which can increase the susceptibility of weld failure due to solidification cracking. Adding sufficient amounts of manganese can reduce the chances of cracking. Instead of FeS formation, the MnS forms at the grain boundaries as globules with high melting points, which make mild steels containing manganese less susceptible to solidification cracking [Ref. 1]. Sulfur is always considered deleterious in steel weldments and, as a result, it is usually kept well below 0.005 wt% in both base plate and weld metal.

Copper may also react with sulfur to produce CuS and/or Cu_2S or Cu(Mn)S complexes. Copper sulfides also form as globules with relatively high melting points, hence rendering the weld metal less susceptible to solidification cracking.

It has been found that manganese and copper sulfides can form complexes with many oxides that nucleate acicular ferrite. The sulfides form as "caps" [Ref. 22, 23] on

the previously nucleated oxides. The issue of whether manganese sulfide effectively promotes acicular ferrite formation is controversial. Yamamoto et al. [Ref. 24] believe that MnS, which has been found to form on titanium oxides, can be responsible for the nucleation of acicular ferrite. However, others, such as Abson [Ref. 25] and Blais et al. [Ref. 26], believe that these "caps" reduce the acicular ferrite forming capability of inclusions because they 'coat' the acicular ferrite forming phases. The discussion of the next section suggests that these sulfides can nucleate acicular ferrite by heterogeneous nucleation but because their crystal structures are not cubic they cannot provide sites for epitaxial growth. In addition, it would seem that sulfides does not react chemically with the surrounding solid steel in a way that titanium-containing oxides appear to do.

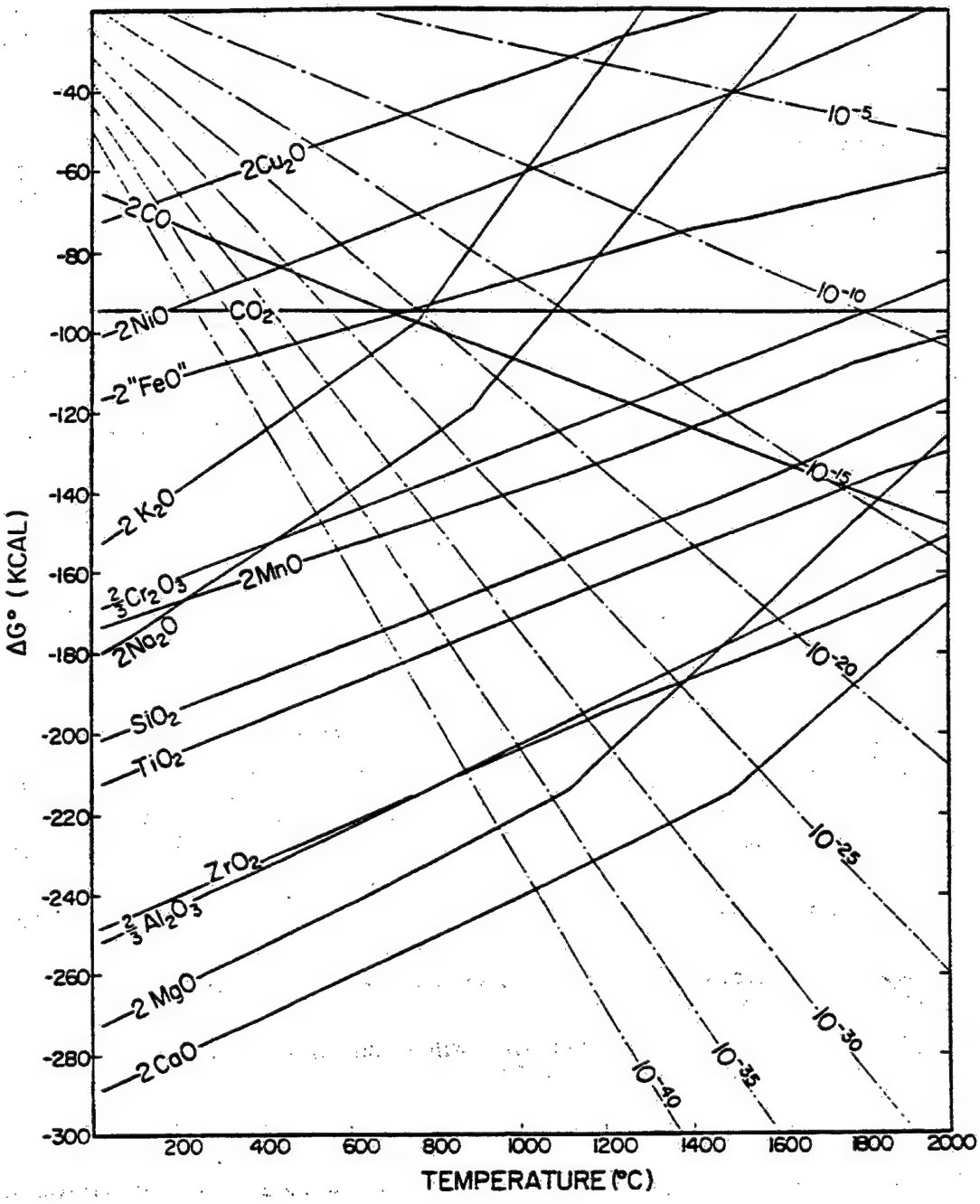

Figure 2-7. Free energy of formation of oxides from [Ref. 27].

D. A DISCUSSION OF PREVIOUS WORK AIMED AT UNDERSTANDING THE NUCLEATION OF ACICULAR FERRITE

1. General

For many years, scientists categorized acicular ferrite and bainite together and, in fact, they have many similarities. Both microstructures are similar, but acicular ferrite is nucleated intragranularly within austenite grains on non-metallic inclusions whereas bainite is nucleated at grain boundaries. Acicular refers to an object pointed like a needle. Acicular ferrite comprises ferrite plates, that appear as needles in two dimensions that form on non-metallic inclusions and these interlock to form a basket-weave microstructure, which greatly enhances the mechanical properties in the weld metal.

Acicular ferrite has been extensively researched to determine how it forms for particular non-metallic inclusions and not for others. The analyses include energy dispersion x-ray (EDX), parallel electron energy loss spectroscopy (PEELS), electron diffraction, and other analytical methods. The results of this work still have not provided a conclusive answer as to why acicular ferrite nucleates on certain non-metallic inclusions and not on others. Several theories have been generated to describe the mechanisms of nucleation of acicular ferrite, but no one theory can be agreed upon. These mechanisms are discussed below.

2. Acicular Ferrite Nucleation Mechanisms

Four possible nucleation mechanisms have been studied over the years to describe the relation between acicular ferrite and non-metallic inclusions. Some researchers believe that more than one mechanism is responsible for acicular ferrite nucleation. These are:

a. Heterogeneous Nucleation by a Simple Substrate

The theory of heterogeneous nucleation is a simple and often thought of as the only growth mechanism. The point of this theory is that the acicular ferrite will nucleate heterogeneously on any type of inclusion, as these lower the free energy barrier to nucleation [Ref.28]. However, calculations based on this theory indicate that inclusions will be less effective at nucleating acicular ferrite than grain boundaries, due to higher curvature at the surface of inclusions than at the grain boundaries [Ref. 8]. Since the energy of formation decreases as the surface area curvature decreases, this would mean that larger inclusions would be more effective at nucleating acicular ferrite. Some workers believe that allotriomorphic ferrite forms along the grain boundaries and this promotes acicular ferrite formation at inclusions since the grain boundary ferrite growth is impeded by increased carbon levels in the austenite at the grain boundary austenite/ferrite interface [Ref. 29].

b. Epitaxy

Epitaxial growth is a very popular theory, which is also known as lattice matching. Epitaxial growth is a process in which the liquid or solid phase arranges atoms crystallographically to a crystalline substrate [Ref. 1]. Lattice matching requires that the non-metallic inclusions have crystal structures orientated in a way to align with the ferrite. The inclusions need to have a cubic crystal structure and have planes, which match appropriate planes in α-ferrite. This lowers the energy of nucleation of the ferrite. Whether or not acicular ferrite will form is dependent on the inclusion crystal structure and its orientation. It has been shown that certain non-metallic inclusions, such as TiO, TiN, γ-Al_2O_3, and $MnO.Al_2O_3$, have cubic crystal structures and good lattice matching

with ferrite (and thus prior austenite) for certain well matched crystal orientations in both the inclusions and ferrite [Ref. 15]. For example, for the epitaxial nucleation of acicular ferrite on γ-Al_2O_3 (corundum) that will be studied in the present work, the (100) plane in the corundum is parallel to the (011) plane in the α-ferrite during epitaxial growth. In addition, the $[01\bar{1}]$ direction in the alumina will be parallel to the $[5\bar{3}3]$ direction in the α-ferrite. The matching of the interplanar spacings between the corundum and the ferrite in this orientation is not usually perfect but shows a disregistry of about 2%. Other inclusions that have potential epitaxial relationships with α-ferrite have often been assessed as to their effectiveness in nucleating acicular ferrite through their calculated values of disregistry [Ref. 15].

c. Strain Energy

As the weld metal solidifies, the difference between the thermal expansion coefficients between the non-metallic inclusions and austenite matrix cause strains around the inclusion. The transformation from austenite to ferrite would seem to relieve these strains [Ref 6, 30, 31]. This theory is popular, but Gregg et al. [Ref. 32] dismiss it on energy grounds (not enough). However, this mechanism could operate in conjunction with others to help provide sufficient energy for acicular ferrite nucleation.

d. Interface Effects

The theory of interface effects considers possible chemical reactions between the non-metallic inclusion and austenite interface. Some research suggests that chemical reaction seems to be more effective at nucleating acicular ferrite rather than strain energy [Ref. 33]. Research conducted by Gregg et al. [Ref. 32] shows that oxidation of the titanium oxides and carbon-oxygen interactions in the prior austenite

matrix can effectively nucleate acicular ferrite. Their research indicates that manganese and carbon are reduced near the inclusion/austenite interfaces, which locally reduces the hardenability of the weld metal so that ferrite nucleation is more readily accomplished.

3. Inclusion Compositions Believed to Form Acicular Ferrite

The determination of non-metallic inclusion chemistry through analytical modeling is extremely difficult. Babu et al. [Ref. 12] have been able to produce time temperature transformation and nucleation rate curves for several inclusion oxides. Even though the model correlates with previous experimental data, the results are based on uniform weld composition. Even though this is actually not the case, they believe that MnO, SiO_2, Ti_3O_5, TiO_2, Al_2O_3, and $MnO.Al_2O_3$ can be responsible for the nucleation of acicular ferrite in C-Mn weld metals containing titanium.

Zhang and Farrar [Ref. 28] claim that the growth mechanism for acicular ferrite for the non-metallic inclusions follows the classical heterogeneous nucleation theory, and that epitaxy, strain, and chemical bonding effects are not significant and so only inclusion size and number is important. They concluded that the inclusions that form acicular ferrite include: TiO, Al_2O_3, SiO_2, $MnO.SiO_2$, TiO $(Al_2O_3).MnO.SiO_2$ complexes, MnS, and CuS, and claimed that all are equally effective at nucleating acicular ferrite provided that they have the same size. They also claim that small amounts of Al_2O_3 and TiO changed the size distribution of the inclusions, so that less acicular ferrite is nucleated because the average size is reduced. They also believe that high weld metal aluminum content increases the soluble aluminum content of the weld metal and that encourages side-plate ferrite formation at the expense of acicular ferrite. However, work by Evans

[Ref. 34] indicates that the ferrite with second phase content scarcely changes with increasing aluminum content in some C-Mn steel weld metals containing acicular ferrite.

Aluminum- and titanium-free C-Mn steel weld metals contain inclusions that are primarily $MnO.SiO_2$. Other phases form as the aluminum content is increased. These include: $3MnO.Al_2O_3.3SiO_2$ (spessartite), $MnO.Al_2O_3.2SiO_2$ (mullite), $MnO.Al_2O_3$ (galaxite), and Al_2O_3. If silicon contents are low, pure Al_2O_3 can form if aluminum contents are high [Ref. 34]. Figure 2-8 is a ternary diagram for the $MnO\text{-}SiO_2\text{-}Al_2O_3$ system. Fox and Brothers [Ref. 19] suggest that both $MnO.Al_2O_3$ (galaxite) and $MnO.TiO_2$ (pyrophanite), if titanium is present, can nucleate acicular ferrite. When titanium is added to aluminum-rich weld metals, very complex inclusion compositions can be obtained, such as $Al_2O_3.TiO$ [Ref. 22] and $MnTi_2O_4$ [Ref. 26]. Greene's work [Ref. 23] suggests that the coordination of titanium in the inclusions in C-Mn steels containing 28 ppm Ti (and no Al) is TiO-like. This was determined by energy-loss near-edge fine structure (ELNES) studies in parallel electron energy loss spectra (PEELS). However, phase diagrams have not yet been developed for these systems, which make them difficult to study.

Titanium oxides, such as TiO, TiO_2, and Ti_2O_3 have been shown to nucleate acicular ferrite [Ref. 13, 16, 17]. Also, Grong et al. [Ref. 15] have found that TiN as well as $\gamma\text{-}Al_2O_3$ and $MnO.Al_2O_3$ (Galaxite) can be responsible for the epitaxial nucleation of acicular ferrite. Both interface chemical reactions and epitaxy have been considered as possible mechanisms by which titanium oxide-containing inclusions nucleate acicular ferrite.

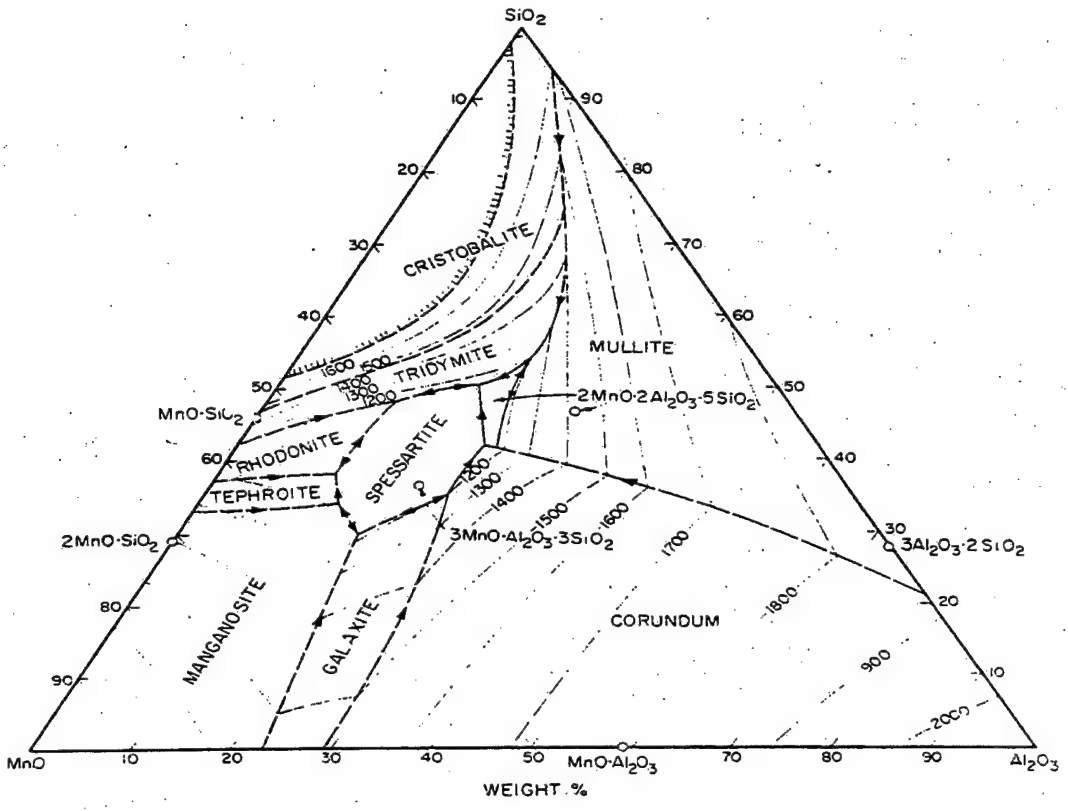

Figure 2-8. Ternary diagram of MnO-SiO_2-Al_2O_3 system from [Ref. 34].

E. SCOPE OF THE PRESENT WORK

It is quite clear that the relationship between non-metallic inclusion and acicular ferrite formation is very complex and not fully understood. In the present study, five titanium-free (<5 ppm) C-Mn steel weldments containing varying amounts of aluminum and different volume percentages of acicular ferrite will be studied. The object of this research is to further the knowledge on the mechanisms responsible for nucleating acicular ferrite by aluminum-containing inclusions.

Scanning electron microscopy (SEM) will be used to measure the size, distribution, and volume fraction of the inclusions present. SEM energy dispersive x-ray (EDX) analysis will be performed to get an estimate of the compositions of the

inclusions. Transmission electron microscopy (TEM) will be conducted using carbon extraction replicas. TEM/EDX spectra and diffraction patterns will be analyzed to determine compositions and phases of the inclusions.

This research will provide definitive data on size and distribution, crystallography, and composition of acicular ferrite forming inclusions in aluminum-deoxidized C-Mn steel weld metals. With the combination of previous work and the results of this research, it is hoped that the exact mechanisms of acicular ferrite formation by inclusions in the $MnO.SiO_2.Al_2O_3$ phase field will be discovered.

III. EXPERIMENTAL PROCEDURE

A. WELD SAMPLE PRODUCTION

Dr. G. M. Evans, in association with Oerlikon Welding Limited, Zurich, Switzerland, prepared the six Shielded Metal Arc Welding samples used in the current study. The only significant difference in each sample was the aluminum composition. The weld sample preparation is covered in Reference 35, and is outlined below.

1. Electrode

Six basic low hydrogen electrodes were used with different amounts of aluminum added to their coatings. The amounts of aluminum varied to obtain the levels of aluminum in the weld metal, shown in Table 3-1. The electrodes were then extruded onto 4 mm core wire. A coating to electrode diameter ratio (D/d) of 1.68 was used. Table 3-2 shows the chemical composition of the six samples studied.

Sample	Al ppm
C2.10	6
C2.11	60
C2.12	150
C2.13	250
C2.14	420
C2.15	660

Table 3-1. Final aluminum content in the weld metal.

Sample	C	Mn	Si	S	P	Ti	B	Al	N	O
	%					ppm				
C2.10	0.074	1.49	0.29	0.006	0.013	5	2	6	72	471
C2.11	0.081	1.43	0.29	0.006	0.013	5	2	60	54	461
C2.12	0.076	1.36	0.34	0.005	0.011	5	2	150	57	476
C2.13	0.079	1.37	0.39	0.005	0.011	5	2	250	47	446
C2.14	0.079	1.40	0.44	0.004	0.011	5	2	420	44	436
C2.15	0.081	1.42	0.48	0.004	0.006	4	2	660	46	444

Table 3-2. Chemical composition of the steel weld metal from [Ref. 35].

2. Weld Preparation

The specification of the joint geometry is located in ISO 2560-1973. Two 20 mm thick plates were welded together with three beads per layer for a total of 27 weld beads required to fill the joint. Each weld was performed in the flat position. The welding parameters were: direct current of 170 Amps, voltage of 21 volts, and nominal heat-input of 1kJ/mm. The interpass temperature was maintained at 200°C.

3. Mechanical Testing

Each welded sample was mechanically tested for yield strength, ultimate strength, percent elongation, reduction of area percentage, and shelf temperatures from Charpy-V notch tests. Approximately thirty-five Charpy-V notch specimens were tested for each sample to obtain a full transition temperature curve. The results of the mechanical properties are shown in Table 3-3.

Sample	YS	UTS	EL	RA	Charpy Test	
	MPa	MPa	%	%	100 J, °F	28 J, °F
C2.10	431	527	29.6	78.0	-19	-41
C2.11	444	542	27.6	72.9	-15	-39
C2.12	437	527	24.6	78.9	-20	-58
C2.13	437	538	25.2	78.9	-25	-56
C2.14	469	545	24.4	77.0	-30	-62
C2.15	466	551	26.2	78.9	-29	-76

Table 3-3. Mechanical properties of the five samples studied from [Ref. 35].

B. SAMPLE PREPARATION

Each of the six weld samples were cut transversely into one-inch specimens for analysis. The following procedure for preparation included: grinding on 400 and 600 grit Struers and Buehler silicon paper, polishing on Buehler Microcloth with 3 μm diamond compound suspended in water, followed by polishing with 1 μm diamond compound.

C. SCANNING ELECTRON MICROSCOPY (SEM)

1. SEM Overview

The Scanning Electron Microscope (SEM) uses an electron beam, which is scanned over the surface of an object with a raster to produce a three-dimensional appearing image. Figure 3-1 is a picture of the Topcon SM-510(a) and the Cambridge S200 (b) used for the current work. The SEM can be used to examine the size and shape of the features on a particular sample, and can estimate the composition using energy dispersive x-ray analysis.

Sample	YS	UTS	EL	RA	Charpy Test	
	MPa	MPa	%	%	100 J, °F	28 J, °F
C2.10	431	527	29.6	78.0	-19	-41
C2.11	444	542	27.6	72.9	-15	-39
C2.12	437	527	24.6	78.9	-20	-58
C2.13	437	538	25.2	78.9	-25	-56
C2.14	469	545	24.4	77.0	-30	-62
C2.15	466	551	26.2	78.9	-29	-76

Table 3-3. Mechanical properties of the five samples studied from [Ref. 35].

B. SAMPLE PREPARATION

Each of the six weld samples were cut transversely into one-inch specimens for analysis. The following procedure for preparation included: grinding on 400 and 600 grit Struers and Buehler silicon paper, polishing on Buehler Microcloth with 3 μm diamond compound suspended in water, followed by polishing with 1 μm diamond compound.

C. SCANNING ELECTRON MICROSCOPY (SEM)

1. SEM Overview

The Scanning Electron Microscope (SEM) uses an electron beam, which is scanned over the surface of an object with a raster to produce a three-dimensional appearing image. Figure 3-1 is a picture of the Topcon SM-510(a) and the Cambridge S200 (b) used for the current work. The SEM can be used to examine the size and shape of the features on a particular sample, and can estimate the composition using energy dispersive x-ray analysis.

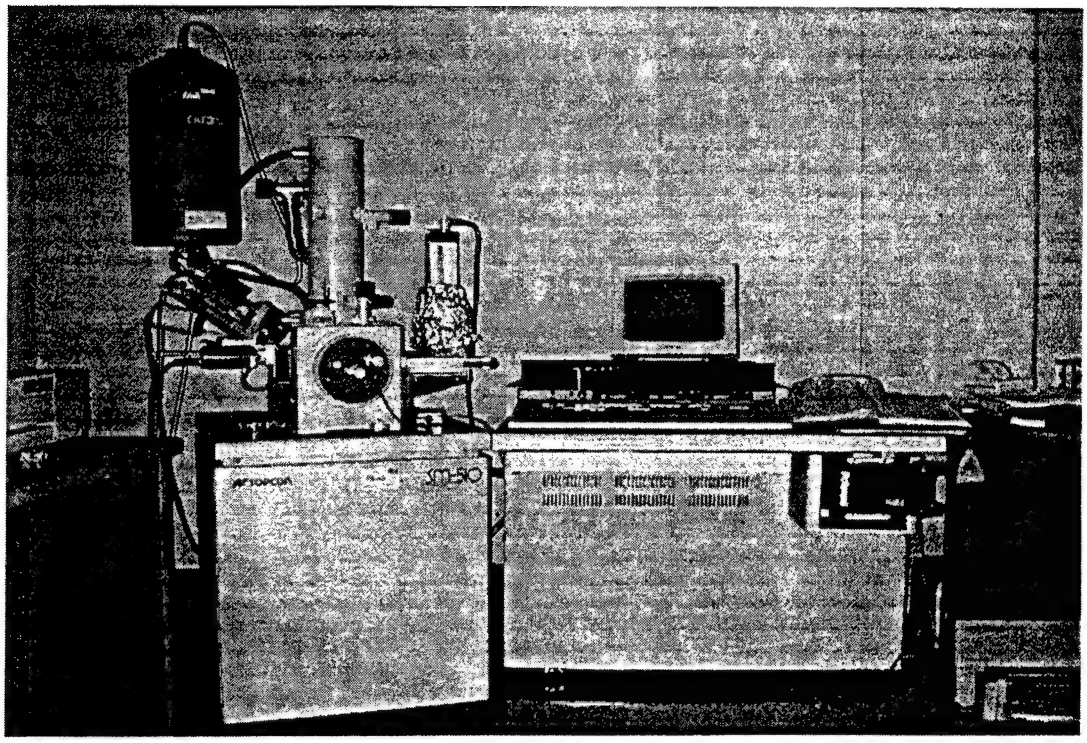

(a)

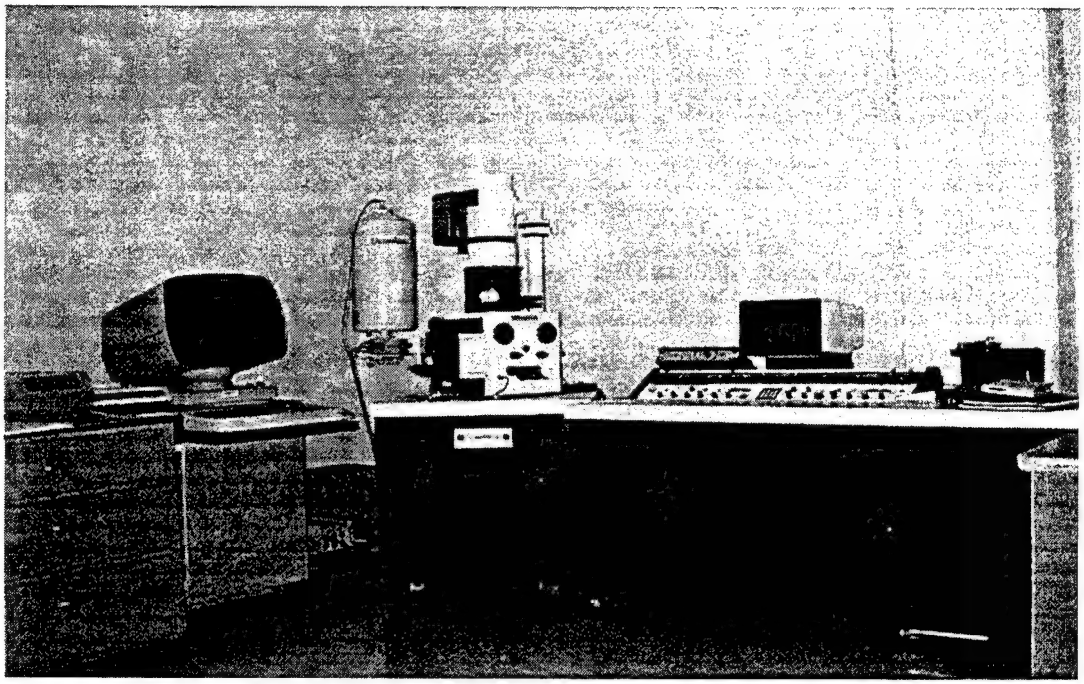

(b)

Figure 3-1. The Topcon SM 510 (a) and Cambridge S200 (b) SEMs at the Naval Postgraduate School.

Figure 3-2 is a schematic diagram of a typical SEM. The major components of the SEM are: 1) an electron gun, which emits a high-intensity electron beam using a tungsten filament in the Topcon SM510 and a LaB_6 filament in the Cambridge S200, 2) a column, which consists of magnetic lenses to focus the electron beam to adequate probe size, 3) a scanning system, which scans the electron beam over a sample, 4) an electron collector and display system, which converts the collected electrons to an image, and 5) control electronics, which controls the above systems.

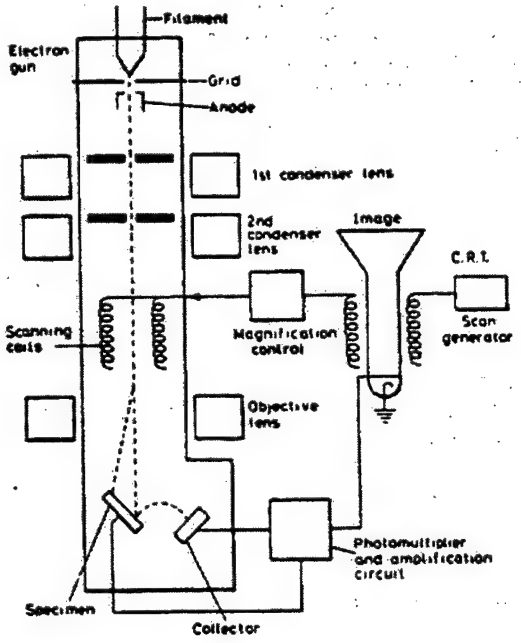

Figure 3-2. A schematic diagram of a typical SEM.

The electrons are accelerated down the column and strike the sample. The electrons interact with the sample and emit Auger electrons, X-rays, back-scattered electrons, and secondary electrons. Figure 3-3 is a schematic of the signals produced in the SEM. One signal not listed is light because it is very hard to detect, and a special

cathodoluminescence detector must be attached to sense it. These signals are processed to produce images and chemical information of the sample.

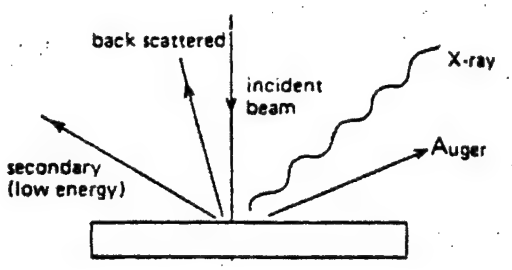

Figure 3-3. Schematic of the signals produced by the SEM

2. Procedure

The objective of using the SEM is to acquire the average size, distribution and volume fraction of inclusions. From this information, an analysis of the size, distribution, and volume fraction of inclusions and the nucleation of acicular ferrite can be made.

In order to analyze the inclusions, the present work used secondary electrons. The difference between secondary electrons and back-scattered electrons is that secondary electrons are emitted closer to the surface of the sample. Back-scattered electrons may include underlying inclusions due to the depth of the electron beam penetration. Figure 3-4 is a schematic diagram of the depths of penetration for various emitted signals. The inclusions are imaged in two-dimensional planar sections from which true inclusion diameters and volume fractions can be obtained by stereological calculations.

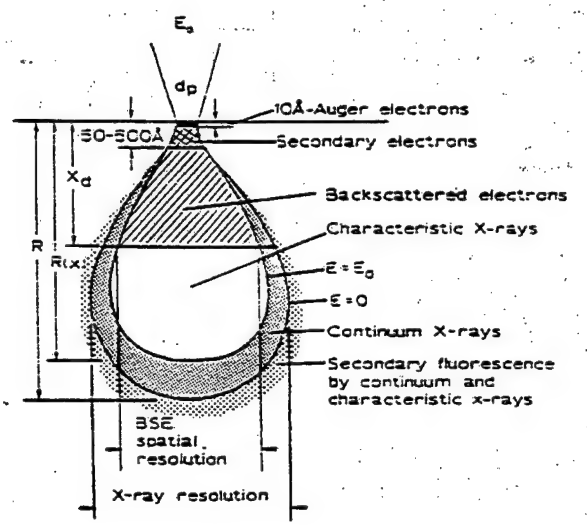

Figure 3-4. Schematic of the depth of penetration for various emitted signals.

The SEM used in this work is the Topcon SM 510, which is connected to a 486/DX2 computer equipped with Link ISIS and Link Tetra software. The microscope settings were 20 kV accelerating voltage, 10 mm working distance, and a magnification of 5000X. One hundred images were taken for each sample in the secondary electron mode. Each field was analyzed for inclusion size, with the minimum size of 0.15 μm measured. These micrographs were also measured for total area of each field (575.7 μm^2). A mean value of the diameter was calculated with a confidence level of 95%.

The confidence level of 95% was calculated using:

$$CI = \pm 1.96\left(\frac{\sigma}{\sqrt{n}}\right)$$

where n is the population and σ is the standard deviation, given by the equation:

$$\sigma = \sqrt{\frac{n\sum x^2 - \left(\sum x\right)^2}{n(n-1)}}$$

where x is the range on either side of the sample mean that 95% of all the data lay. The distribution of the size of inclusions is the statistical representation of the percentage of inclusions that lay between the ranges of diameters.

From the mean diameter measured in a planar section and number of inclusions per field, the volume fraction was calculated. From Fullman [Ref. 36], the true average particle size (diameter) is:

$$\overline{D_V} = \frac{\pi \overline{D}_A}{2}$$

where $\overline{D_A}$ is the average diameter measured in area. This equation takes into account that the inclusions are not sectioned across the middle (necessarily). The number of particles per unit volume, N_V, is:

$$N_V = \frac{N_A}{\overline{D_A}}$$

where N_A is the number of inclusion measured per unit area. With a little bit of algebra, the equation for volume fraction, V_f, is given by:

$$V_f = \frac{N_A \pi^3 \overline{D}_A^{\,2}}{24}$$

This calculation incorporates the stereology of the inclusions. The spheres are not sectioned directly in the center so averages have to be used. In previous work by Mahoney [Ref. 37], he assumed that the area fraction, A_f, is equal to the volume fraction. However, this assumption would only be correct if all the inclusions were cut across an equator during sectioning and polishing. The expression for area fraction, A_f, is

$$A_f = \frac{N_A \pi \overline{D}_A^2}{4} = \frac{V_f}{1.645}$$

D. TRANSMISSION ELECTRON MICROSCOPY (TEM)

The non-metallic inclusions were analyzed using the transmission electron microscope with energy dispersive x-ray microanalysis and diffraction analysis. The TEM is the most powerful tool to analyze the morphology, chemistry and crystallography of samples. In the present work carbon extraction replicas were made from each sample and analyzed for chemical composition and diffraction patterns to investigate and determine the mechanisms that affect acicular nucleation in aluminum-rich steel weld metals.

1. TEM Overview

The transmission electron microscope is used for studying thin samples vice bulk samples in the SEM. The TEM uses higher voltages, has a lower limit of spatial resolution, and can thus achieve higher magnifications. The resolving power is so good that atomic resolution is possible. The present work used the Topcon 002B TEM, Figure 3-5. This TEM has a LaB_6 crystal that is energized to 200,000 volts, providing electrons at very small wavelengths. The limit of resolution (Scherzer) for this microscope is approximately 0.18 nm. The chemical analysis and scanning transmission electron microscopy imaging used a probe size of 4.7 nm and 2.5 nm, respectively, in the present work.

The TEM system consists of an electron gun, a complex system of condenser lenses, and a complex system of objective, projector and intermediate lenses. Due to the possibility of electrons being scattered by air molecules, a vacuum system must be used in the column. The electron gun emits electrons through the column, which are then collimated through the condenser lenses to the sample. The sample is usually a thin foil or a carbon extraction replica (used in the present work). The electrons pass through the sample and the image is magnified and focused through the objective lenses to produce a final image. Objective apertures are used to limit defects in the lenses and selected area diffraction apertures to produce diffraction patterns. The images produced on a fluorescent screen or with the screen removed, they can be collected digitally by computer. Figure 3-6 shows a schematic diagram of how images and diffraction patterns are formed on the fluorescent screen.

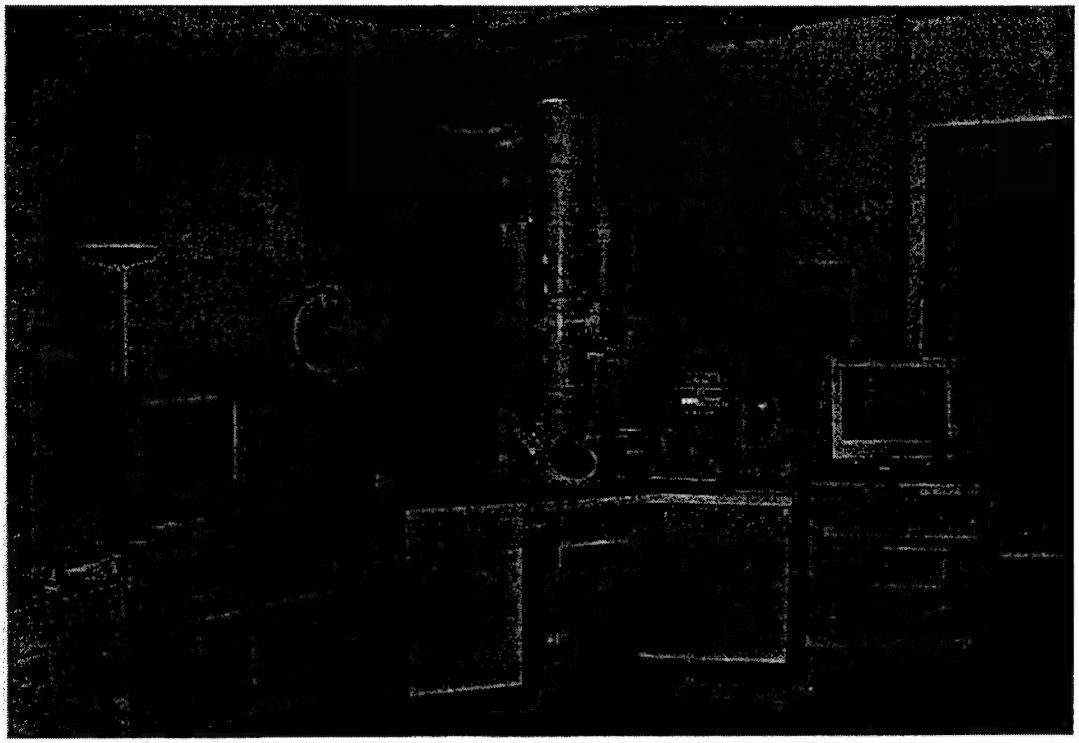

Figure 3-5. Picture of the Topcon 002B TEM at the Naval Postgraduate School.

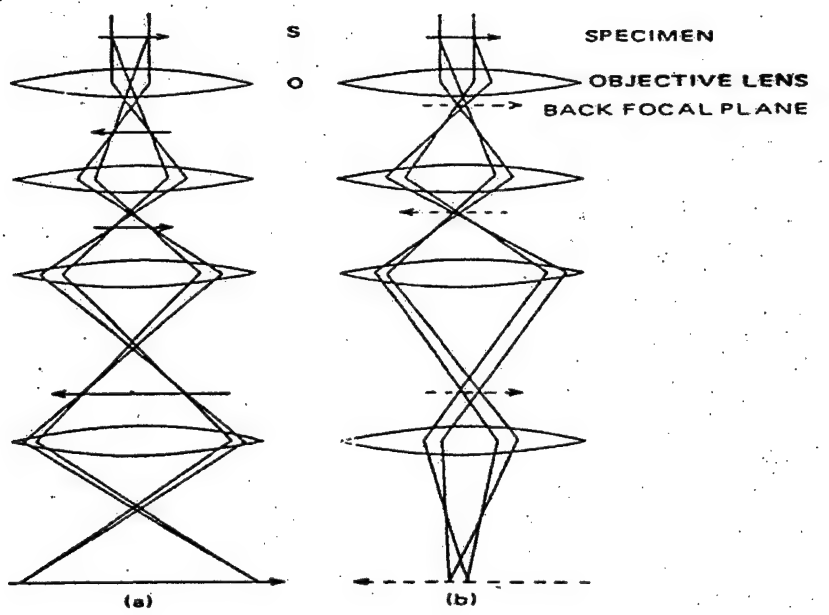

Figure 3-6. Schematic of how images (a) and diffraction patterns (b) are produced.

2. Carbon Extraction Replicas

Carbon extraction replicas were made for each of the six samples in the present work. Each weld sample was repolished and etched in a 5% nital and 95% methanol solution for twenty seconds, to expose the inclusions on the surface. Each sample was masked with tape to only expose the last weld pass. After placing the samples into the vacuum chamber of the Ernest F. Fullman Mk II carbon coater, three carbon strands were wound together and placed between the electrodes. The distance between the carbon fibers and the sample was 3.1 cm. The vacuum chamber was evacuated to 200 μTorr. A current was then applied to the carbon fibers until the carbon was extracted from the fibers. The carbon deposits itself on the exposed area of the sample. The process is repeated until a layer of approximately 200 nm, a bluish-gray color, was deposited on the

sample. The sample was then removed from the chamber and the tape removed. The carbon deposit was scribed into 3mm squares. The samples were placed into the 5% nital bath to deep etch. This deep etch enabled the scribed regions to float off or partially peel off the surface. The carbon extractions were carefully lifted out of the nital solution and placed into a 5% acetone water bath to flatten the samples (surface tension effect). It also makes it easier to lift the extractions, containing the non-metallic inclusions, with 400-mesh nickel grid. Due to the possible presence of copper sulfides in the non-metallic inclusions, the nickel grids were chosen so accurate assessments of the sulfides could be made.

3. Energy Dispersive X-ray (EDX) Spectroscopy

As the electron beam passes through the non-metallic inclusions, characteristic x-rays for elements are emitted and detected by the energy dispersive x-ray detector. The electron beam interacts with the electron shells in the atoms, causing characteristic x-rays to be emitted. The EDX detector, which is made of lithium drifted silicon, measures these energies and sends the results to a computer. The number of counts of particular x-ray energies can allow quantification of the sample. This is achieved by the analysis of the counts versus energy spectrum.

In order to aid in this process, the present work used a computer software program, ESVision, from EMISPEC Inc. The software takes the intensities of the x-rays and the characteristic x-ray information and produces the spectrum. The integrated intensities of the characteristic lines in this spectrum are measured to obtain the chemical composition of the inclusions. One problem with EDX is that light elements, such as oxygen, are usually difficult to detect because they are absorbed and have a low

fluorescent yield, and thus are hard to detect. However, in the present study, the stoichiometric composition of the oxides is known so the amount of oxygen need not be calculated from first principles. The oxide compositions can thus be determined by the atomic percentages of the elements.

4. Diffraction

Bragg diffraction of electrons creates diffraction patterns, which can be analyzed to determine the crystallography of the material studied. The electron beam is scattered at small angles as it passes through the sample, producing a Laué spot pattern for crystalline material. Measuring the Bragg diffraction angles and the wavelength of the electrons, determination of the Bravais lattice of the inclusion crystal structure can be made. Diffraction patterns and EDX data are powerful tools to characterize the phases in the inclusion. However, most inclusions that nucleate acicular ferrite are usually multiphase and polycrystalline so analysis can be difficult. The present work analyzed the diffraction patterns to determine if they were crystalline or amorphous. Amorphous structures display diffuse ring patterns as compared with crystalline structures which produce Laué spot patterns.

THIS PAGE INTENTIONALLY LEFT BLANK

IV. RESULTS AND ANALYSIS

A. INTRODUCTION

It is clear from the background section that the effect of the deoxidation elements manganese, silicon, aluminum and titanium on the chemistry and crystallography of the inclusions present in C-Mn steel weld metal is very important. In a classic work, Kluken and Grong [Ref. 38] investigated the size distribution and chemistry in C-Mn welds deoxidized with varying amounts of all four elements in the hope of understanding how acicular ferrite was nucleated in these weld metals. It was clear from this work that high levels of acicular ferrite could be obtained by carefully controlling the titanium and aluminum contents of the weld metals, but the exact mechanism of nucleation was not discovered, although Grong et al [Ref. 15] did subsequently show that the cubic inclusions, γ-Al_2O_3, $MnO.Al_2O_3$ (galaxite) and TiN could nucleate acicular ferrite by epitaxy. Blais et al. [Ref. 26] studied very similar weldments for which only manganese, silicon, and titanium were used as deoxidants, and suggested that titanium-containing oxides, including $MnO.Ti_2O_3$ and TiO, could nucleate acicular ferrite although they were not sure by which mechanism: they did however suggest that chemical reaction between titanium-containing oxide inclusions and the prior austenite could be responsible.

Mahoney [Ref. 37] and Walters [Ref. 22] studied carefully chosen weld metals with almost identical chemistry in which the titanium and aluminum contents were varied in a closely controlled way and found that TiO and $TiO.Al_2O_3$, Al_2O_3 and TiN could all be responsible for acicular ferrite nucleation in agreement with Grong and co-workers [Ref. 15] and Blais et al. [Ref. 26].

In the present work, weld metals from the same source (Dr. G. M. Evans) as all these previous workers was studied. In this case, however, only manganese, silicon, and aluminum were present as deoxidants (titanium < 5 ppm). This was done with a view to completing the inclusion story for these C-Mn weld metals so that a complete understanding of the nature of acicular ferrite in these could hopefully be established. As a result a careful comparison of the results of the present work with those of Grong and co-workers, Blais et al., and Walters and Mahoney will be made.

B. WELD COMPOSITION

Dr. G. M. Evans [Ref. 35] provided the six weld metal samples and their chemical composition. Table 4-1 is the chemical composition of the six weld metal samples studies. All elements with the exception of aluminum were held constant. The typical errors in the chemical analysis for the elements in wt% are: Mn-0.02, Si-0.01, Al and P-0.002, C, S, Ti, O, N and B-0.001. Table 4-2 contains the chemical composition of the samples examined by Mahoney [Ref. 37]. Table 4-3 contains the chemical composition of the samples examined by Blais [Ref. 26]. Samples for both the sets of work were also provided by Dr. G. M. Evans [Ref. 35].

Sample	C	Mn	Si	S	P	Ti	B	Al	N	O
	wt%					ppm				
C2.10	0.074	1.49	0.29	0.006	0.013	5	2	6	72	471
C2.11	0.081	1.43	0.29	0.006	0.013	5	2	60	54	461
C2.12	0.076	1.36	0.34	0.005	0.011	5	2	150	57	476
C2.13	0.079	1.37	0.39	0.005	0.011	5	2	250	47	446
C2.14	0.079	1.40	0.44	0.004	0.011	5	2	420	44	436
C2.15	0.081	1.42	0.48	0.004	0.006	4	2	660	46	444

Table 4-1. Chemical composition of the steel weld metal from [Ref. 35].

Sample	C	Mn	Si	S	P	Ti	B	Al	N	O
	wt%					Ppm				
O	0.074	1.4	0.25	0.008	0.007	1	1	6	79	475
W	0.077	1.46	0.27	0.008	0.007	28	3	5	81	459
Y	0.07	1.57	0.45	0.006	0.01	390	39	13	83	308
Z	0.072	1.56	0.49	0.007	0.01	420	48	160	67	438
V	0.078	1.44	0.6	0.006	0.007	540	56	580	41	336

Table 4-2. Chemical composition of the steel weld metal for samples in Mahoney work.

Sample	C	Mn	Si	S	P	Ti	N	O
	wt%							
O	0.074	1.4	0.25	0.008	0.007	0.0001	0.0079	0.048
W	0.077	1.46	0.27	0.008	0.007	0.0028	0.0081	0.046
R	0.074	1.45	0.3	0.007	0.009	0.012	0.0084	0.034
X	0.069	1.47	0.45	0.005	0.006	0.041	0.0077	0.028

Table 4-3. Chemical composition of the steel weld metal for samples in Blais' work.

C. ACICULAR FERRITE IN THE WELD METAL

Evans used reference 3 to identify the microstructure of each of the weld metal samples through the use of manual point count survey. He used optical microscopy of the last weld pass bead to quantify and determine the major microstructural components as described previously. The results showed that sample C2.10, which is aluminum- and titanium-free, to have the lowest amount of acicular ferrite, 9%. The other samples contain between 10 to 22 % acicular ferrite. It should be noted from Table 3-3 that the mechanical properties of the weld metals are significantly improved by increasing acicular ferrite content. Figure 4-1 shows graphically the percentage of acicular ferrite with respect to aluminum content in the weld metal for the samples studied in the present work. Figure 4-2 shows graphically the percentage of acicular ferrite with respect to

titanium content in the weld metal for the samples studied by Blais et al [Ref. 26]. Figure 4-3 shows graphically the percentage of acicular ferrite with respect to (a) titanium content and (b) aluminum content in the weld metal for the samples studied by Mahoney [Ref. 37]. The data in the present work indicates an increase in the aluminum content in the weld metal leads to an increase in the amount of acicular ferrite from 9% (6 ppm Al) to 22% (660 ppm Al). From Blais et al. and Mahoney, the data clearly shows greater amounts of acicular ferrite (between 70 and 90%), where the inclusions contain large amounts of titanium oxides.

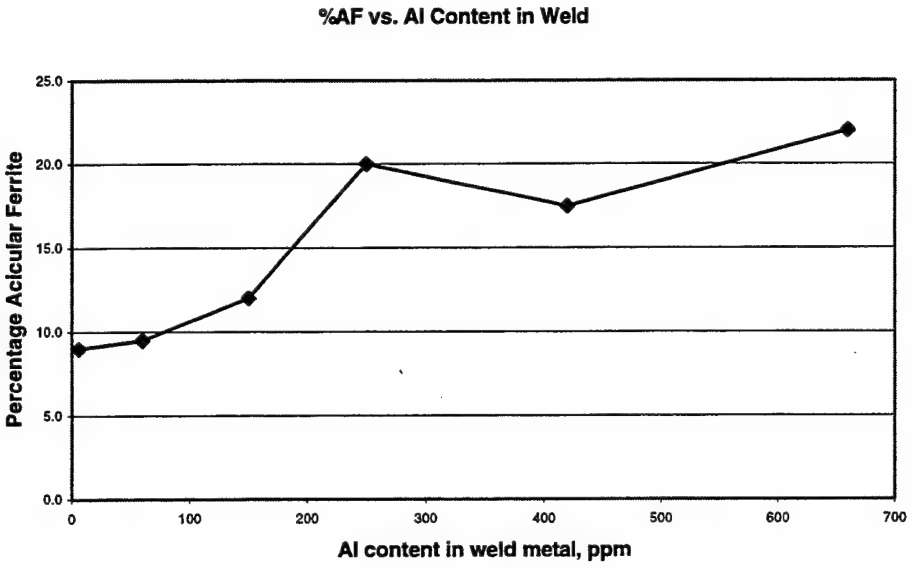

Figure 4-1. Percentage of acicular ferrite versus aluminum content in the weld in present work.

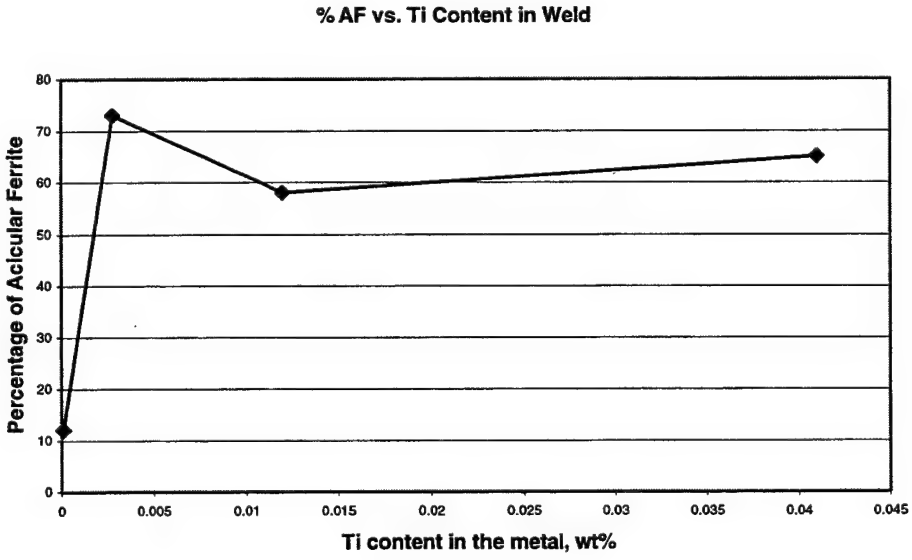

Figure 4-2. Percentage of acicular ferrite versus titanium content in the weld by Blais et al. from [Ref. 26].

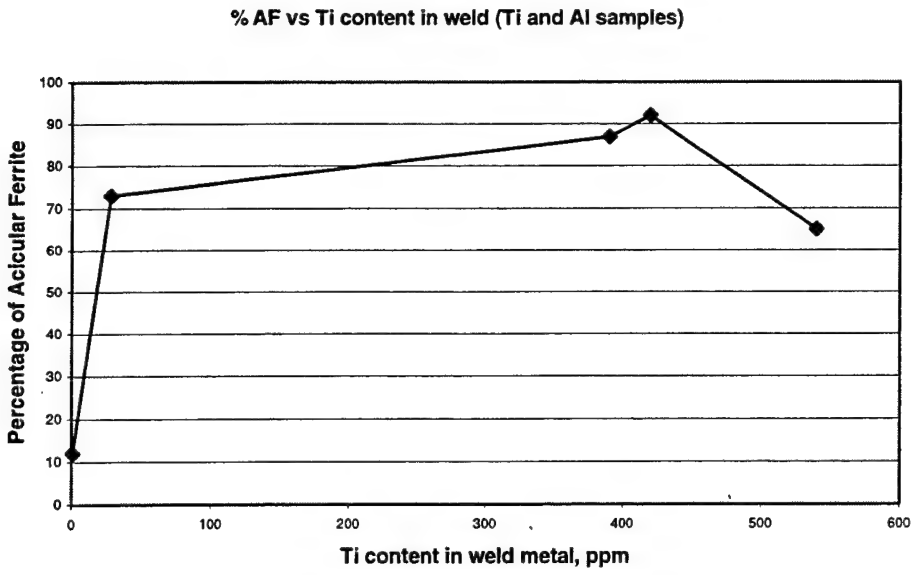

(a)

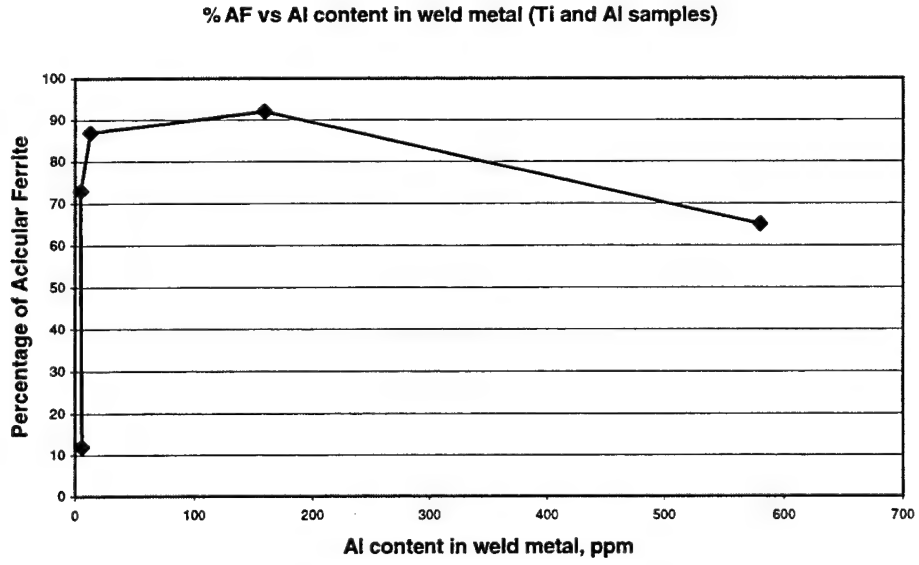

(b)

Figure 4-3. (a) Percentage of acicular ferrite versus titanium content in the weld and (b) percentage of acicular ferrite versus aluminum in the weld by Mahoney from [Ref. 37].

D. INCLUSION SIZE DISTRIBUTION AND VOLUME FRACTION

1. Size Distribution and Previous Research Conversion

Each sample was measured for the average size and number of inclusions using the SEM. The average sizes measured were area diameters, which does not take into account that the spherical inclusions were not necessarily sectioned directly across their centers. The volume fraction was thus calculated as described in the last section. Table 4-4 shows the results of the volume fraction, inclusion size, and number of inclusions for each of the six samples. The volume fractions calculated by Mahoney [Ref. 37] are actually area fractions and need to be converted into volume fractions by multiplication by a factor of $\pi^2/6$ for comparison with the present work. Also, the diameters measured by Mahoney were area diameters. To convert his diameters to volume diameters, the area diameters must be multiplied by a factor of 1.57 as discussed in Section III.C.2. The data determined by Blais [Ref. 26] (deoxidized with Ti (Mn and Si) only) will be assumed to be correct since there is no information as to how the calculations for mean diameter and volume fraction were determined. Tables 4-5 and 4-6 show the data scaled from Mahoney's thesis [Ref. 37] and the data provided by Blais [Ref. 26]. Kluken and Grong [Ref. 38] performed excellent research that incorporated the theory that the spherical particles are not sectioned in the middle. Their inclusion size data also correlates well with the current research. The problem with their work is they took into account too many experimental variables to allow them to perform a complete analysis. They did not control the specific elements, titanium, aluminum, manganese and silicon, separately so that they could analyze the effects of titanium (manganese and silicon) alone or aluminum (manganese and silicon) alone or titanium and aluminum (manganese and

silicon). It must be said, however, that this was not the main aim of Kluken and Grong's work.

Sample Al only									
Sample	# Inclusions	Area Mean Dia(μm)	Vol. Mean Dia(μm)	+/- CI	% A.F.	Af (avg)	Vf (avg)	Vf error w/std dev	Vf (theory)
C2:10	1688	0.3625	0.5691	0.008789	9.0	0.003026	0.004977	0.000241	0.2357
C2:11	1435	0.3487	0.5475	0.005304	9.5	0.002380	0.003916	0.000119	0.2307
C2:12	1101	0.3545	0.5566	0.008414	12.0	0.001888	0.003106	0.000147	0.2381
C2:13	894	0.3392	0.5325	0.008095	20.0	0.001403	0.002308	0.000110	0.2231
C2:14	703	0.3310	0.5197	0.008576	17.5	0.001051	0.001729	0.000090	0.2181
C2:15	634	0.3315	0.5205	0.012591	22.0	0.000951	0.001564	0.000119	0.2221

Table 4-4. Average inclusion size and volume fraction for the six samples.

Sample	Af Ti+Al (Meas.)	Vf Ti+Al (Actual)	Vf error (Ti+Al)	Area Mean Dia., μm	Vol. Mean Dia., μm
	0.00287	0.004721	0.00043	0.3033	0.4762
	0.00148	0.002435	0.00021	0.2405	0.3776
	0.00069	0.001135	0.00006	0.2047	0.3214
	0.0007	0.001152	0.00009	0.2154	0.3382
	0.00071	0.001168	0.00010	0.2406	0.3777

Table 4-5. Average inclusion sizes and volume fractions from Mahoney from [Ref. 37]

Sample	Vf Ti only	Vol. Diam. (μm)
	0.0022	0.34
	0.0023	0.32
	0.0016	0.31
	0.002	0.35

Table 4-6. Average inclusion sizes and volume fractions from Blais from [Ref. 26].

The size distributions of the inclusions for each sample were analyzed. Inclusions less than 0.15 μm in area diameter proved difficult to measure in the SEM. The size distributions for the mean area diameter are shown in Figures 4-4 through 4-6. These diameters were then converted into volume diameters by multiplying them by a factor of 1.57 in the manner previously discussed.

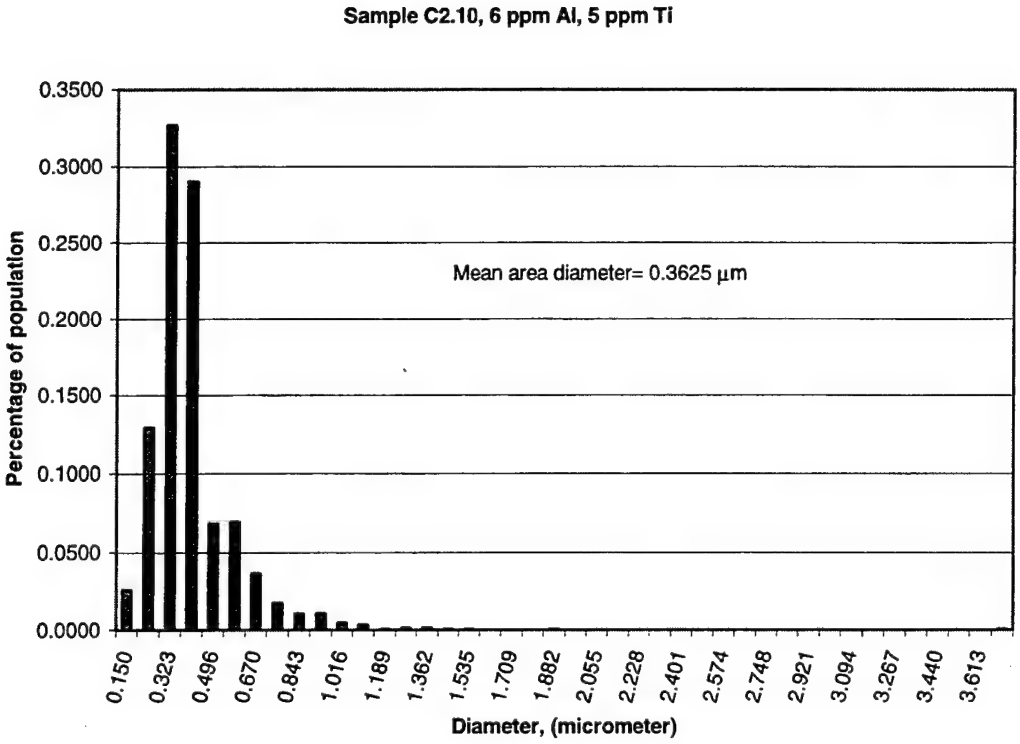

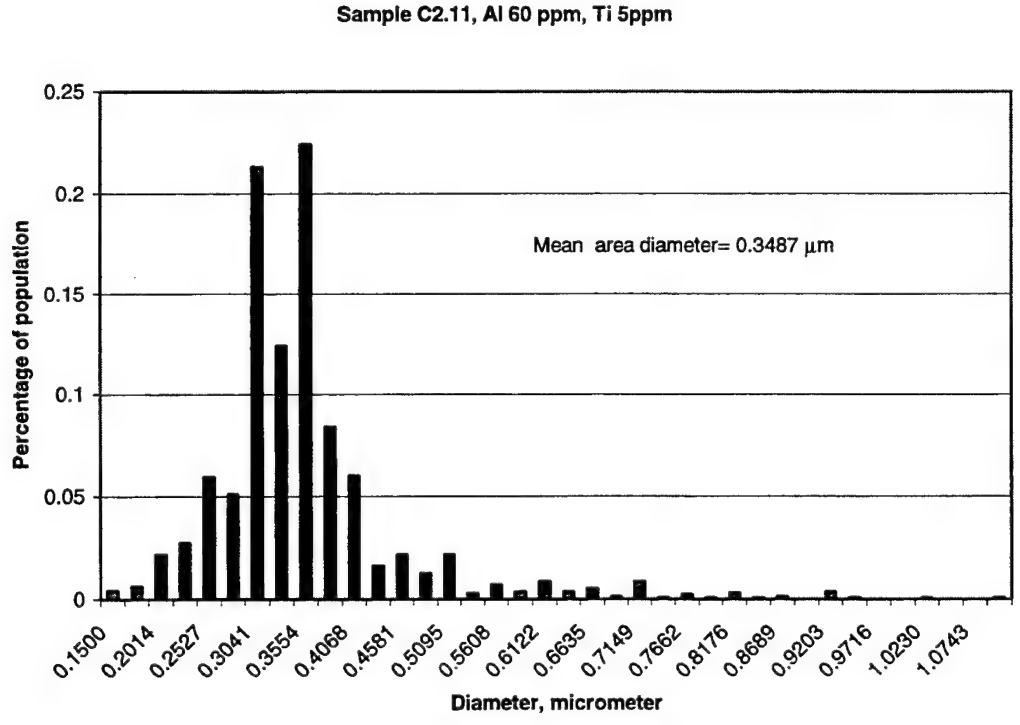

Figure 4-4. Size distribution for samples C2.10 and C2.11.

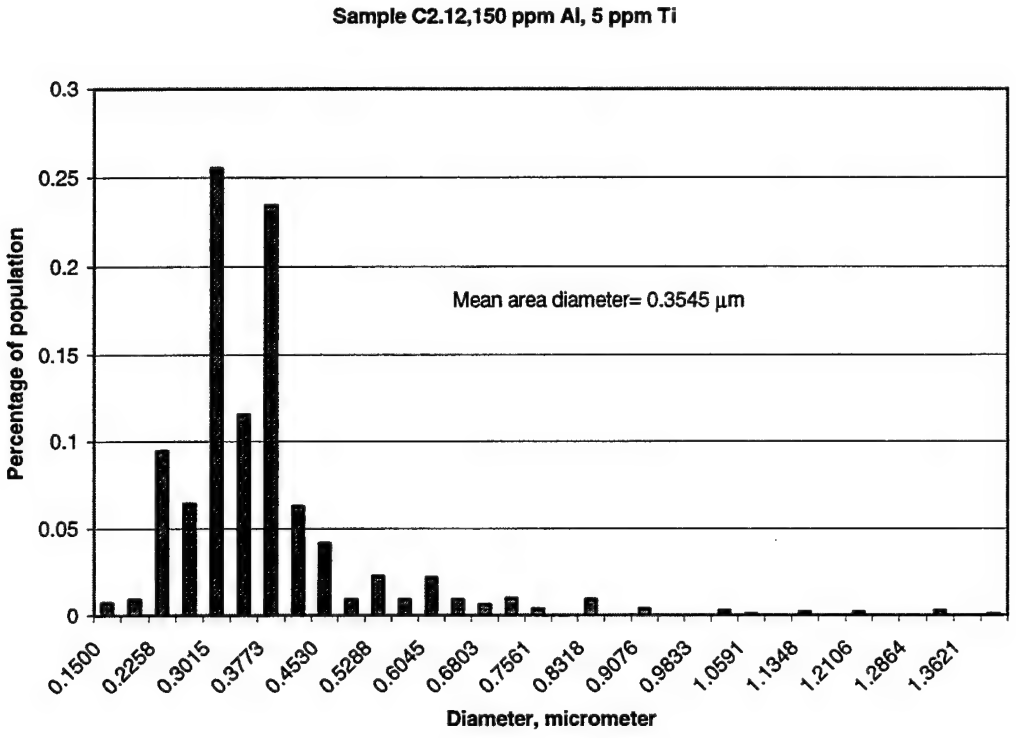

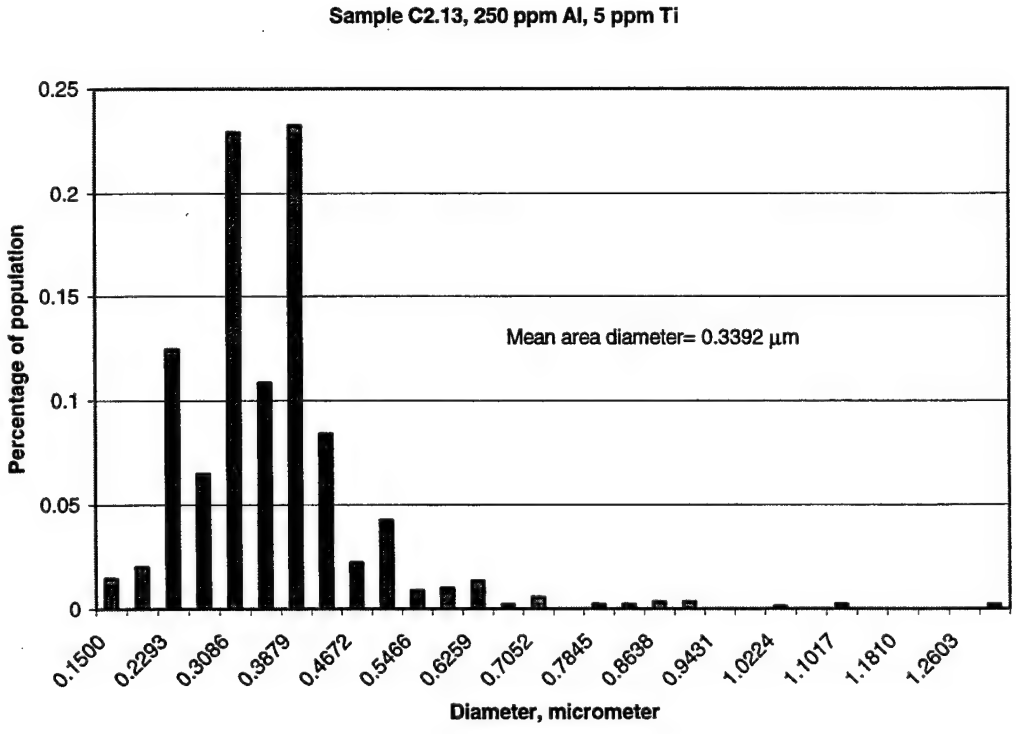

Figure 4-5. Size distribution for samples C2.12 and C2.13.

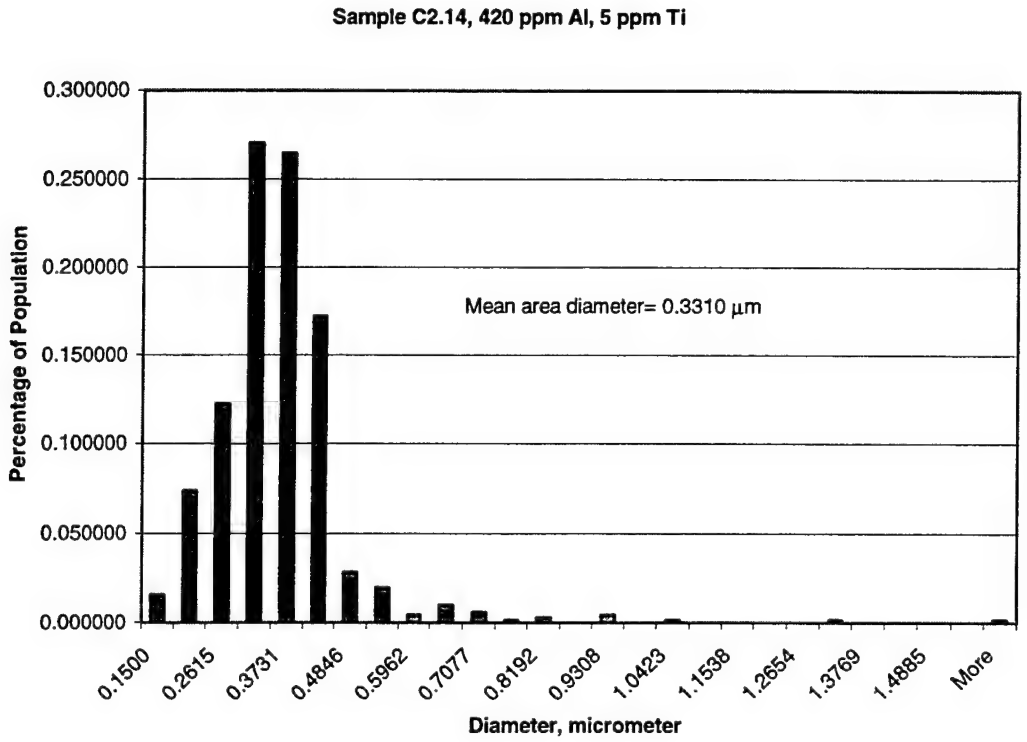

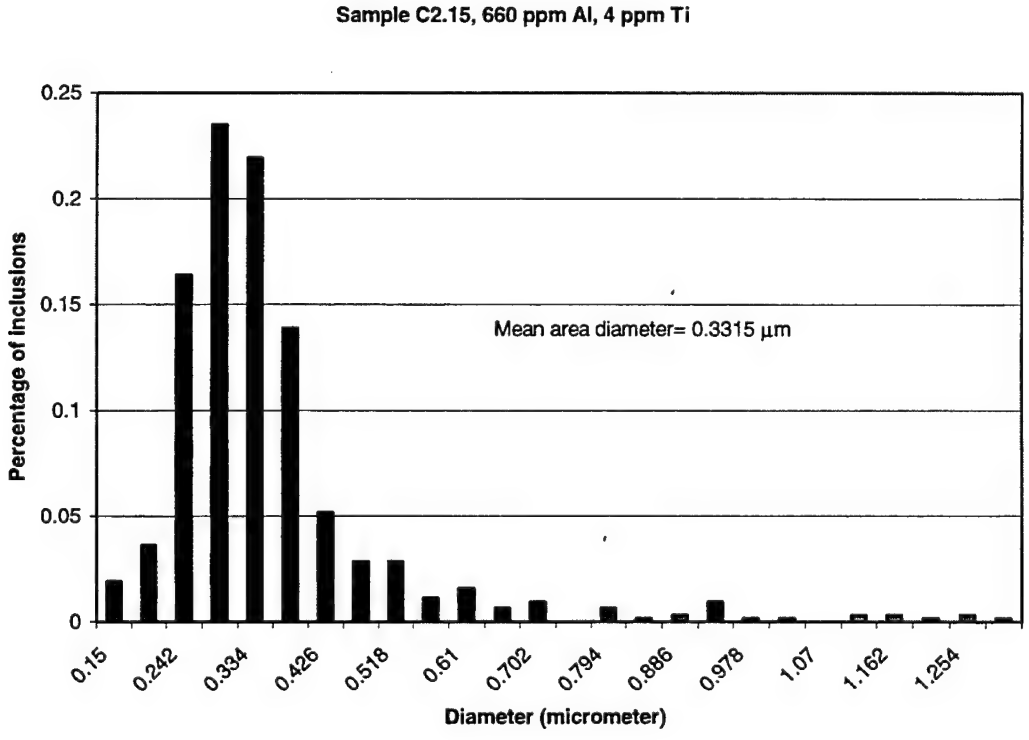

Figure 4-6. Size distribution for samples C2.14 and C2.15.

Figure 4-7 is a graph of the percentage of acicular ferrite versus the volume diameter of the inclusions (present work). Even though it is observed that the average inclusion sizes are the same size within experimental error, Figure 4-7 clearly suggests that there is an increase of acicular ferrite as the diameters get smaller. This contradicts the assertion of Zhang and Farrar [Ref. 28], who claim that as inclusions increase in size, the inclusion will more readily nucleate acicular ferrite. As it can be assumed that the inclusions are the same size within experimental error, this suggests that the increase of acicular ferrite has to be nucleated by a mechanism other than simple heterogeneous nucleation..

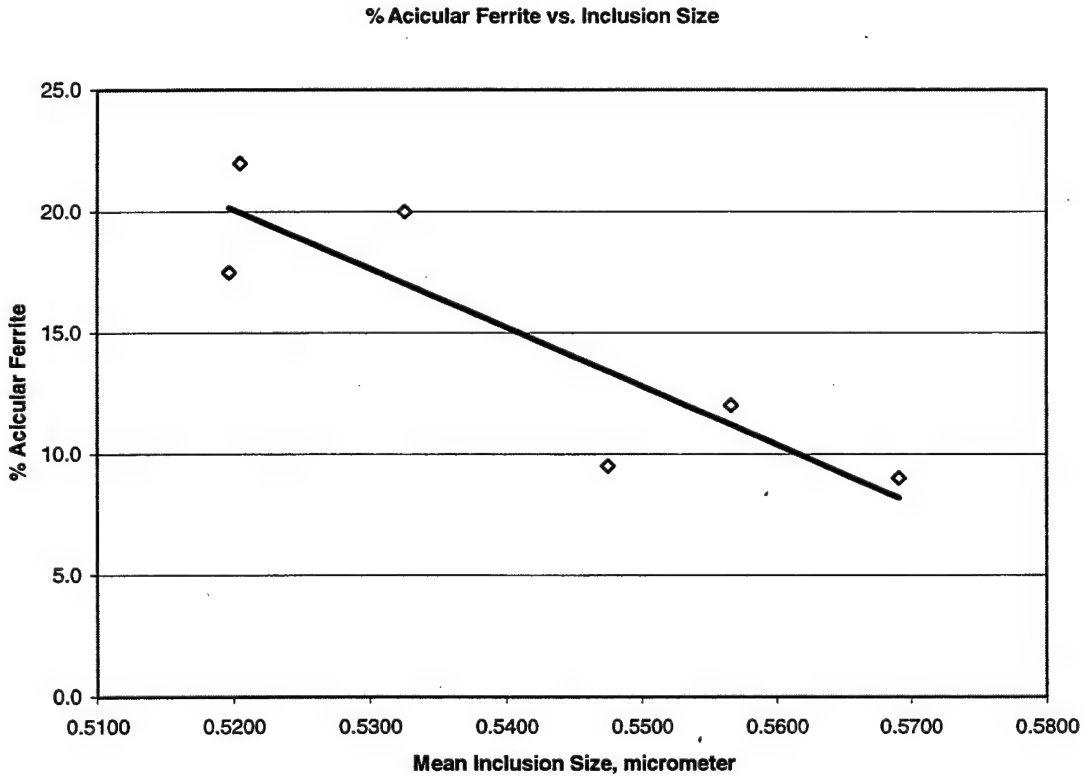

Figure 4-7. Graph of acicular ferrite versus mean inclusion size.

In addition, it has been observed that the inclusion size increases as the oxygen content in the weld metal increases. This can be seen in Figure 4-8. The titanium-only samples and the titanium plus aluminum samples also follow these trends. This data was taken from the previous research from Blais [Ref. 26] and Mahoney [Ref. 37], discussed previously. It should be noted that deoxidation by a combination of titanium and aluminum leads to significantly lower inclusion sizes than those obtained by deoxidation with aluminum (manganese and silicon) alone or titanium (manganese and silicon) alone.

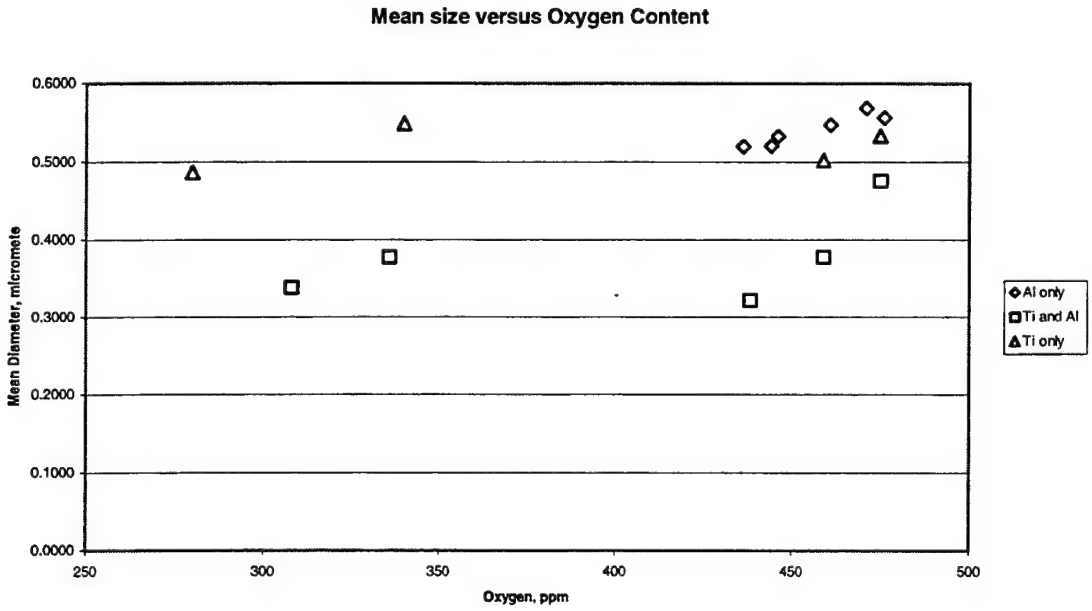

Figure 4-8. Graph of mean diameter versus oxygen content in the weld.

2. Volume Fraction

In previous work, some researchers have cited results for volume fraction, assuming that the area fraction is equal to volume fraction. However, according to Fullman [Ref. 36], this cannot be true as the inclusions being sectioned across planes that do not necessarily pass through the middle of them. To compare the present work results

to this previous work, their volume fractions had to be scaled. One such comparison is the volume fraction versus the oxygen content in the weld metal. Figure 4-9 is a graph of the volume fraction from the present and previous work versus the oxygen content in the weld. Figure 4-10 shows the same graph as Figure 4-9 with the theoretical values calculated using the method of Franklin [Ref. 39].

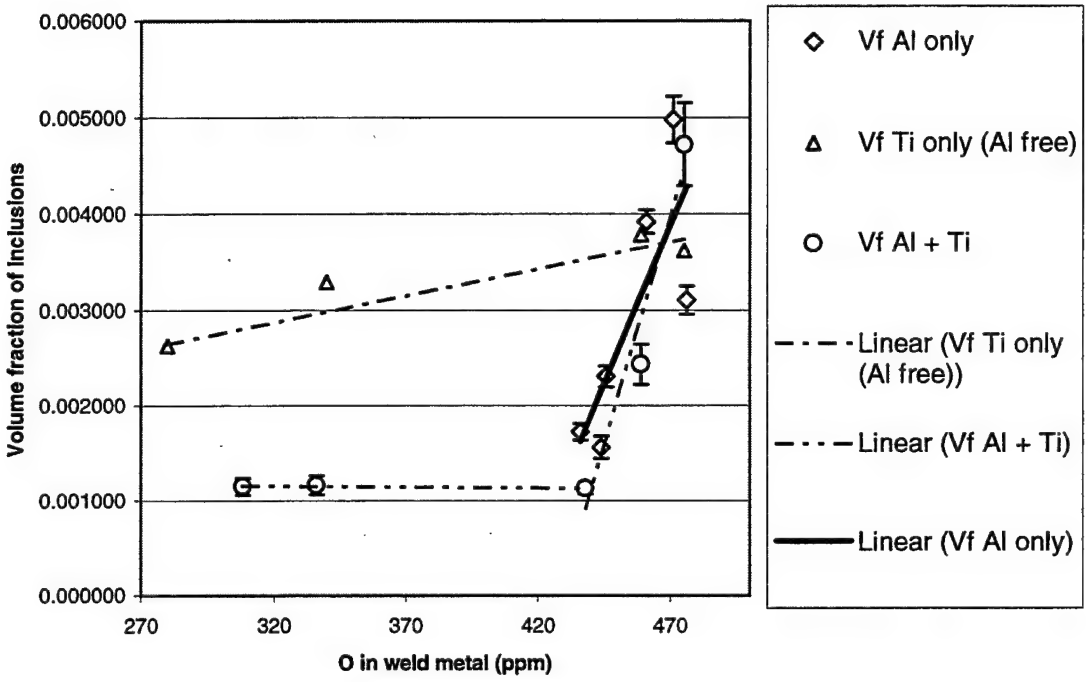

Figure 4-9. Graph of volume fraction vs. oxygen content in the weld metal.

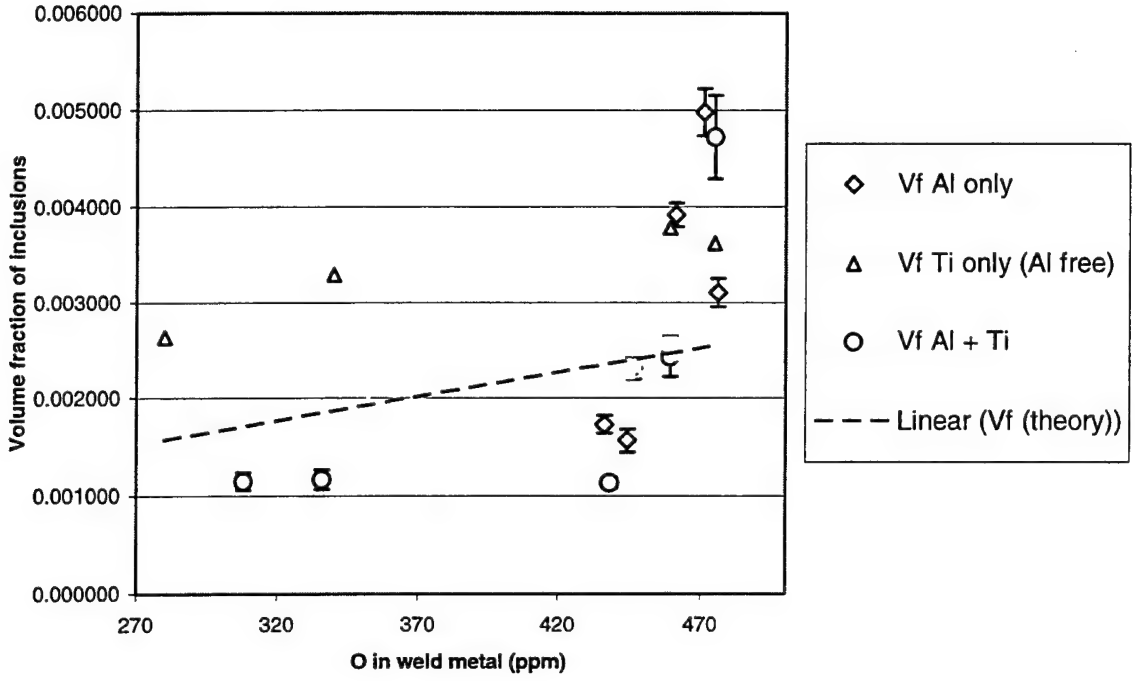

Figure 4-10. Graph of volume fraction versus oxygen content of the weld metal. The theoretical line calculated using the model of Franklin from [Ref. 39]is superimposed.

Using Figure 4-9, some conclusions can be made concerning the effects of the deoxidant additions on volume fraction and oxygen content in the weld metal. Adding increasing amounts of titanium decreases the amount of oxygen in the weld metal, but does not lower the volume fraction of inclusions particularly rapidly. The gradient of the linear fit to this titanium data suggests that the ratio between the oxygen content of the inclusions and the dissolved oxygen is not changing rapidly, if at all. On the other hand, adding increasing amounts of aluminum only to weld metals (without titanium) significantly decreases the volume fraction of inclusions, but the total oxygen content does not appear to change much. This implies that there is more dissolved oxygen in the weld metal rather than in the inclusions as the aluminum content increases. The reason

for this is likely to be that, as the weld metal aluminum increases, there is more dissolved aluminum in the weld metal and thus the dissolved oxygen in the weld metal increases because oxygen atoms like to associate with aluminum atoms because aluminum is a strong deoxidizer. Thirdly, increasing the amounts of titanium and aluminum together has a two-fold effect. First, the volume fraction decreases rapidly, so there are less inclusions but the dissolved oxygen is still high. Secondly, the increases of titanium and aluminum then apparently reduce the dissolved oxygen content of the weld metal as well. Finally, Kluken and Grong [Ref. 38] have suggested that the inclusion volume fraction for steels containing manganese and silicon but no aluminum and titanium can be determined by the approximate formula of Franklin [Ref. 39],

$$V_f = 0.05 * w_O + 0.054\left(w_S - w_S^{sol}\right)$$

where V_f is the theory volume fraction, w_O is the oxygen content in wt%, w_S is the sulfur content in wt%, and w_S^{sol} is the soluble sulfur content (assumed to be 0.003 wt%). This theoretical volume fraction was plotted in Figure 4-10 for the oxygen content in the present work, and is represented by the dashed line. These simple theoretical values have the right order of magnitude but unfortunately cannot accurately predict the effects the trace deoxidants have on the weld metal inclusion behavior.

The current work indicates that smaller inclusion volume fractions can promote the nucleation of acicular ferrite. The reason for this will be discussed shortly. This is in contrast to (the assertion made by) Zhang and Farrar [Ref. 28] as their assessment of inclusion behavior suggests that increasing numbers of inclusions would lead to increased amounts of acicular ferrite. Adding aluminum to the weld metal has a dual effect on the strength and toughness of the weld metal. The first effect is the number and size of

inclusions are reduced so less sites for crack initiation are present. The second effect is that more acicular ferrite forms, which improves toughness. Consequently, in contrast to popular belief, increasing amounts of aluminum can be beneficial for improving the toughness of weld metal, even if the dissolved aluminum increases the hardenability, since acicular ferrite can be nucleated rather than Widmanstätten ferrite.

E. TEM/EDX RESULTS

Each weld metal sample had a carbon extraction replica made in order to study the non-metallic inclusions. These replicas were used to determine the chemical composition using EDX. Also, the non-metallic inclusions were studied to determine whether they were facetted or entirely spherical and whether they were crystalline or glassy from the diffraction patterns. The TEM was the primary instrument used to determine these features. However, the Cambridge S200 SEM was used to get a preliminary estimate for the inclusion composition. The SEM/EDX does not give very accurate results for inclusion composition, as they are rather small (~0.5 μm diameter) with volumes that are somewhat less than the volume of interaction between the electron beam and the (nominally) infinitely thick sample.

1. Chemical Composition

The chemical composition of the inclusions for each weld sample was investigated by using Energy Dispersive X-ray Spectroscopy. The chemical composition of twenty inclusions per sample was made with the exception of sample C2.15, which clearly showed that the oxide component of the inclusions were very close-to pure Al_2O_3 within experimental error. The quantification of the inclusion EDX spectra resulted in

atomic percentage of each element, normalized to 100%. Light elements such as oxygen were not analyzed directly because the oxygen content could be determined accurately from stoichiometry, so that the weight percent of the oxides could be determined. The results of the analysis are displayed in Tables 4-7 through 4-12. It should be noticed that, in addition to MnO-Al_2O_3-SiO_2 ternary oxide components, the inclusions often contained Cu(Mn)S sulfides that were usually present as "caps" on the oxide component of the inclusions. This suggests that these sulfide phases nucleated on the previously developed oxide components of the inclusions. Their sulfide morphologies and chemistries have been observed previously by several groups of workers [Ref. 15, 22, 23]. The carbon extraction replicas were also placed in the Cambridge S200 SEM, using thin foil conditions in the EDX software, for preliminary chemical analysis. These results of the oxide part of the analysis are compared with the equivalent results of samples studied by Kluken and Grong [Ref. 38], (and also reported in Evans book [Ref. 35]), (varying aluminum while titanium content remains constant at approximately 40 ppm) and are plotted on the ternary diagram in Fig. 4-11.

The MnO-SiO_2-Al_2O_3 ratios of the present work compares well with those of Kluken and Grong (Evans). Their data was obtained using a SEM/EDX system, STEM/EDX, and SEM/WDX. Our TEM/EDX data agrees closely with this data as shown in Figure 4.11. The data from the SEM in the present work is somewhat different. This is due to the thickness and absorption corrections not being made and the samples being too thin for SEM work. Since the inclusion size for the six samples are relatively the same, this data suggests that the higher concentration of aluminum in the inclusions

causes acicular ferrite to nucleate by a different mechanism rather than heterogeneous nucleation as reported by Zhang and Farrar [Ref. 28].

It was also observed that the three samples that contain the most amounts of acicular ferrite (17-22%) lie within the corundum region of the phase diagram. It is well known that corundum has a cubic crystal lattice (distorted spinel). Since ferrite also has a cubic crystal structure, this strongly supports the idea that acicular ferrite is nucleated by epitaxy (good lattice matching) on the γ-Al_2O_3 inclusions in these samples. This will be discussed further in the next section.

Sample C2.10						Inclusion Compound Composition at%						Inclusion Compound Composition wt%					
	Al Ka	Si Ka	S Ka	Mn Ka	Cl Ka	Al_2O_3	SiO_2	MnO	MnS	CuS	CuO	Al_2O_3	SiO_2	MnO	MnS	CuS	CuO
Inclusion	at%	at%	at%	at%	at%	at%	at%	at%	at%	at%	at%	wt%	wt%	wt%	wt%	wt%	wt%
1	2.93	50.27	4.89	38.9	3.01	2.98	61.38	31.66	1.53	2.45	0.00	4.60	55.83	34.01	2.02	3.55	0.00
2	2.15	47.2	5.47	40.48	4.69	2.25	59.28	33.89	0.65	3.93	0.00	3.70	57.49	38.81	0.86	5.66	0.00
3	2.42	49.36	7.5	36.35	4.38	2.50	61.23	30.06	2.58	3.62	0.00	4.20	60.64	35.15	3.38	5.22	0.00
4	1.61	49.52	5.29	42.1	1.48	1.63	60.06	34.04	3.08	1.20	0.00	2.68	58.30	39.02	4.08	1.74	0.00
5	4.44	48.02	4.91	41.16	1.47	4.49	58.25	33.29	2.78	1.19	0.00	7.24	55.39	37.37	3.63	1.70	0.00
6	3.47	53.67	0.62	41.75	0.49	3.41	63.28	32.82	0.10	0.39	0.00	5.37	58.69	35.94	0.14	0.56	0.00
7	2.3	46.78	7.69	41.23	2	2.36	57.53	33.80	4.67	1.64	0.00	3.94	56.71	39.35	6.10	2.35	0.00
8	3.02	52.87	1.34	41.08	1.7	3.00	63.01	32.64	0.00	1.06	0.29	4.77	59.09	36.14	0.00	1.56	0.35
9	1.29	52	3.13	41.36	2.23	1.30	62.85	33.33	0.73	1.80	0.00	2.11	60.20	37.69	0.97	2.64	0.00
10	1.77	49.06	5.42	41.58	2.17	1.80	59.93	33.86	2.65	1.77	0.00	2.97	58.20	38.83	3.50	2.57	0.00
11	2.09	49.84	5.22	41.34	1.5	2.11	60.32	33.36	3.00	1.21	0.00	3.46	58.40	38.13	3.97	1.76	0.00
12	1.53	52.2	2.31	41.74	2.21	1.54	63.01	33.59	0.08	1.78	0.00	2.48	59.85	37.67	0.11	2.61	0.00
13	1.73	51.6	2.94	41.77	1.95	1.74	62.28	33.61	0.80	1.57	0.00	2.81	59.36	37.83	1.06	2.30	0.00
14	2.81	51.34	4.67	38.87	2.3	2.83	62.07	31.33	1.91	1.85	0.00	4.63	59.76	35.62	2.52	2.69	0.00
15	1.7	50.92	3.93	41.16	2.29	1.72	61.80	33.30	1.33	1.85	0.00	2.80	59.40	37.80	1.76	2.71	0.00
16	1.35	52.19	2.37	41.87	2.22	1.36	63.03	33.71	0.12	1.79	0.00	2.19	59.95	37.86	0.16	2.63	0.00
17	1.19	50.94	3.71	41.41	2.75	1.21	62.11	33.66	0.78	2.24	0.00	1.97	59.77	38.25	1.04	3.28	0.00
18	2.2	54.7	0.87	40.23	2	2.16	64.59	31.67	0.00	0.68	0.89	3.48	61.13	35.39	0.00	1.01	1.09
19	2.46	50.15	5	40.63	1.76	2.48	60.70	32.78	2.61	1.42	0.00	4.06	58.58	37.36	3.45	2.06	0.00
20	1.53	53.12	2.31	40.75	2.29	1.53	63.92	32.69	0.02	1.84	0.00	2.48	60.81	36.72	0.02	2.71	0.00
Average	2.20	50.79	3.98	40.79	2.24	2.22	61.55	32.95	1.46	1.75	0.06	3.62	59.05	37.33	1.94	2.55	0.07

Table 4-7. Chemical analysis of twenty inclusions and conversions into oxides for sample C2.10.

Sample C2.11						Inclusion Compound Composition at%						Inclusion Compound Composition wt%					
	Al Ka	Si Ka	S Ka	Mn Ka	Cu Ka	Al_2O_3	SiO_2	MnO	MnS	CuS	CuO	Al_2O_3	SiO_2	MnO	MnS	CuS	CuO
Inclusion	at%	at%	at%	at%	at%	at%	at%	at%	at%	at%	at%	wt%	wt%	wt%	wt%	wt%	wt%
	8.83	36.09	4.02	47.45	3.61	9.46	46.41	40.68	0.35	3.09	0.00	13.85	40.03	41.43	0.44	4.25	0.00
	9.95	35.03	5.89	42.79	6.33	10.90	46.05	37.50	0.00	5.16	0.39	17.00	42.31	40.69	0.00	6.99	0.43
	15.85	37.5	0.24	44.72	1.69	16.18	45.93	36.51	0.00	0.20	1.18	23.57	39.42	37.01	0.00	0.26	1.32
	10.23	37.42	4.58	40.67	7.1	10.96	48.10	34.85	0.00	3.93	2.16	17.24	44.60	38.16	0.00	5.34	2.44
	9.77	37.14	6.15	36.21	10.73	10.63	48.50	31.52	0.00	5.35	3.99	17.39	46.74	35.87	0.00	7.25	4.49
	11.55	36.77	4.4	37.33	9.95	12.35	47.19	31.94	0.00	3.76	4.75	19.80	44.58	35.62	0.00	5.07	5.32
	10.48	42.3	0.09	43.76	3.37	10.59	51.30	35.38	0.00	0.07	2.65	16.19	46.20	37.62	0.00	0.10	3.06
	11.71	40.6	1.57	45.03	1.1	11.98	49.86	36.87	0.38	0.90	0.00	17.88	43.84	38.28	0.48	1.24	0.00
	6.71	37.63	3.68	45.37	6.6	7.18	48.33	38.84	0.00	3.15	2.50	11.46	45.43	43.12	0.00	4.37	2.89
	9.99	36.16	2.71	45.94	5.2	10.59	46.02	38.98	0.00	2.30	2.11	16.34	41.83	41.83	0.00	3.14	2.40
	11.07	41.67	5.07	37.69	4.5	11.62	52.48	31.65	0.48	3.78	0.00	18.00	47.90	34.10	0.60	5.17	0.00
	7.78	34.75	3.76	45.93	7.78	8.42	45.11	39.75	0.00	3.25	3.48	13.43	42.43	44.14	0.00	4.46	3.97
	8.18	28.05	1.65	47.61	14.5	8.94	36.78	41.61	0.00	1.44	11.23	15.01	36.38	48.61	0.00	1.94	12.58
	11.06	44.18	5.39	34.79	4.58	11.49	55.10	28.93	0.67	3.81	0.00	17.94	50.66	31.40	0.84	5.23	0.00
	11.78	43.08	4.26	37.76	3.11	12.13	53.24	31.11	0.95	2.56	0.00	18.62	48.15	33.22	1.18	3.51	0.00
	10.87	43.88	2.35	40	2.9	11.11	53.82	32.70	0.00	1.92	0.45	16.94	48.36	34.70	0.00	2.66	0.52
	9.44	35.52	3.6	45.08	6.37	10.13	45.72	38.69	0.00	3.09	2.38	15.83	42.11	42.07	0.00	4.21	2.70
	10.41	41.04	3.85	40.95	3.75	10.90	51.57	34.30	0.08	3.14	0.00	16.73	46.64	36.63	0.10	4.32	0.00
	9.72	43.97	2.79	41.05	2.46	9.96	54.09	33.66	0.27	2.02	0.00	15.27	48.84	35.89	0.34	2.81	0.00
	10.08	39.04	6.23	39.22	5.43	10.81	50.22	33.63	0.69	4.66	0.00	16.94	46.38	36.68	0.85	6.35	0.00
Average	10.27	38.59	3.61	41.97	5.55	10.84	48.86	35.42	0.20	2.85	1.83	16.86	44.79	38.34	0.24	3.90	2.09

Table 4-8. Chemical analysis of twenty inclusions and conversions into oxides for sample C2.11.

Sample C.2.10						Inclusion Compound Composition at%						Inclusion Compound Composition wt%					
	Al Ka	Si Ka	S Ka	Mn Ka	Cu Ka	Al_2O_3	SiO_2	MnO	MnS	CuS	CuO	Al_2O_3	SiO_2	MnO	MnS	CuS	CuO
Inclusion	at%	at%	at%	at%	at%	at%	at%	at%	at%	at%	at%	wt%	wt%	wt%	wt%	wt%	wt%
1	2.93	50.27	4.89	38.9	3.01	2.98	61.38	31.66	1.53	2.45	0.00	4.60	55.83	34.01	2.02	3.55	0.00
2	2.15	47.2	5.47	40.48	4.69	2.25	59.28	33.89	0.65	3.93	0.00	3.70	57.49	38.81	0.86	5.66	0.00
3	2.42	49.36	7.5	36.35	4.38	2.50	61.23	30.06	2.58	3.62	0.00	4.20	60.64	35.15	3.38	5.22	0.00
4	1.61	49.52	5.29	42.1	1.48	1.63	60.06	34.04	3.08	1.20	0.00	2.68	58.30	39.02	4.08	1.74	0.00
5	4.44	48.02	4.91	41.16	1.47	4.49	58.25	33.29	2.78	1.19	0.00	7.24	55.39	37.37	3.63	1.70	0.00
6	3.47	53.67	0.62	41.75	0.49	3.41	63.28	32.82	0.10	0.39	0.00	5.37	58.69	35.94	0.14	0.56	0.00
7	2.3	46.78	7.69	41.23	2	2.36	57.53	33.80	4.67	1.64	0.00	3.94	56.71	39.35	6.10	2.35	0.00
8	3.02	52.87	1.34	41.08	1.7	3.00	63.01	32.64	0.00	1.06	0.29	4.77	59.09	36.14	0.00	1.56	0.35
9	1.29	52	3.13	41.36	2.23	1.30	62.85	33.33	0.73	1.80	0.00	2.11	60.20	37.69	0.97	2.64	0.00
10	1.77	49.06	5.42	41.58	2.17	1.80	59.93	33.86	2.65	1.77	0.00	2.97	58.20	38.83	3.50	2.57	0.00
11	2.09	49.84	5.22	41.34	1.5	2.11	60.32	33.36	3.00	1.21	0.00	3.46	58.40	38.13	3.97	1.76	0.00
12	1.53	52.2	2.31	41.74	2.21	1.54	63.01	33.59	0.08	1.78	0.00	2.48	59.85	37.67	0.11	2.61	0.00
13	1.73	51.6	2.94	41.77	1.95	1.74	62.28	33.61	0.80	1.57	0.00	2.81	59.36	37.83	1.06	2.30	0.00
14	2.81	51.34	4.67	38.87	2.3	2.83	62.07	31.33	1.91	1.85	0.00	4.63	59.76	35.62	2.52	2.69	0.00
15	1.7	50.92	3.93	41.16	2.29	1.72	61.80	33.30	1.33	1.85	0.00	2.80	59.40	37.80	1.76	2.71	0.00
16	1.35	52.19	2.37	41.87	2.22	1.36	63.03	33.71	0.12	1.79	0.00	2.19	59.95	37.86	0.16	2.63	0.00
17	1.19	50.94	3.71	41.41	2.75	1.21	62.11	33.66	0.78	2.24	0.00	1.97	59.77	38.25	1.04	3.28	0.00
18	2.2	54.7	0.87	40.23	2	2.16	64.59	31.67	0.00	0.68	0.89	3.48	61.13	35.39	0.00	1.01	1.09
19	2.46	50.15	5	40.63	1.76	2.48	60.70	32.78	2.61	1.42	0.00	4.06	58.58	37.36	3.45	2.06	0.00
20	1.53	53.12	2.31	40.75	2.29	1.53	63.92	32.69	0.02	1.84	0.00	2.48	60.81	36.72	0.02	2.71	0.00
Average	2.20	50.79	3.98	40.79	2.24	2.22	61.55	32.95	1.46	1.75	0.06	3.62	59.05	37.33	1.94	2.55	0.07

Table 4-7. Chemical analysis of twenty inclusions and conversions into oxides for sample C2.10.

Sample C.2.11						Inclusion Compound Composition at%						Inclusion Compound Composition wt%					
	Al Ka	Si Ka	S Ka	Mn Ka	Cu Ka	Al_2O_3	SiO_2	MnO	MnS	CuS	CuO	Al_2O_3	SiO_2	MnO	MnS	CuS	CuO
Inclusion	at%	At%	at%	At%	at%	at%	at%	at%	at%	at%	at%	wt%	wt%	wt%	wt%	wt%	wt%
1	8.83	36.09	4.02	47.45	3.61	9.46	46.41	40.68	0.35	3.09	0.00	13.85	40.03	41.43	0.44	4.25	0.00
2	9.95	35.03	5.89	42.79	6.33	10.90	46.05	37.50	0.00	5.16	0.39	17.00	42.31	40.69	0.00	6.99	0.43
3	15.85	37.5	0.24	44.72	1.69	16.18	45.93	36.51	0.00	0.20	1.18	23.57	39.42	37.01	0.00	0.26	1.32
4	10.23	37.42	4.58	40.67	7.1	10.96	48.10	34.85	0.00	3.93	2.16	17.24	44.60	38.16	0.00	5.34	2.44
5	9.77	37.14	6.15	36.21	10.73	10.63	48.50	31.52	0.00	5.35	3.99	17.39	46.74	35.87	0.00	7.25	4.49
6	11.55	36.77	4.4	37.33	9.95	12.35	47.19	31.94	0.00	3.76	4.75	19.80	44.58	35.62	0.00	5.07	5.32
7	10.48	42.3	0.09	43.76	3.37	10.59	51.30	35.38	0.00	0.07	2.65	16.19	46.20	37.62	0.00	0.10	3.06
8	11.71	40.6	1.57	45.03	1.1	11.98	49.86	36.87	0.38	0.90	0.00	17.88	43.84	38.28	0.48	1.24	0.00
9	6.71	37.63	3.68	45.37	6.6	7.18	48.33	38.84	0.00	3.15	2.50	11.46	45.43	43.12	0.00	4.37	2.89
10	9.99	36.16	2.71	45.94	5.2	10.59	46.02	38.98	0.00	2.30	2.11	16.34	41.83	41.83	0.00	3.14	2.40
11	11.07	41.67	5.07	37.69	4.5	11.62	52.48	31.65	0.48	3.78	0.00	18.00	47.90	34.10	0.60	5.17	0.00
12	7.78	34.75	3.76	45.93	7.78	8.42	45.11	39.75	0.00	3.25	3.48	13.43	42.43	44.14	0.00	4.46	3.97
13	8.18	28.05	1.65	47.61	14.5	8.94	36.78	41.61	0.00	1.44	11.23	15.01	36.38	48.61	0.00	1.94	12.58
14	11.06	44.18	5.39	34.79	4.58	11.49	55.10	28.93	0.67	3.81	0.00	17.94	50.66	31.40	0.84	5.23	0.00
15	11.78	43.08	4.26	37.76	3.11	12.13	53.24	31.11	0.95	2.56	0.00	18.62	48.15	33.22	1.18	3.51	0.00
16	10.87	43.88	2.35	40	2.9	11.11	53.82	32.70	0.00	1.92	0.45	16.94	48.36	34.70	0.00	2.66	0.52
17	9.44	35.52	3.6	45.08	6.37	10.13	45.72	38.69	0.00	3.09	2.38	15.83	42.11	42.07	0.00	4.21	2.70
18	10.41	41.04	3.85	40.95	3.75	10.90	51.57	34.30	0.08	3.14	0.00	16.73	46.64	36.63	0.10	4.32	0.00
19	9.72	43.97	2.79	41.05	2.46	9.96	54.09	33.66	0.27	2.02	0.00	15.27	48.84	35.89	0.34	2.81	0.00
20	10.08	39.04	6.23	39.22	5.43	10.81	50.22	33.63	0.69	4.66	0.00	16.94	46.38	36.68	0.85	6.35	0.00
Average	10.27	38.59	3.61	41.97	5.55	10.84	48.86	35.42	0.20	2.85	1.83	16.86	44.79	38.34	0.24	3.90	2.09

Table 4-8. Chemical analysis of twenty inclusions and conversions into oxides for sample C2.11.

	Sample C.2.12					Inclusion Compound Composition at%						Inclusion Compound Composition wt%					
	Al Ka	Si Ka	S Ka	Mn Ka	Cu Ka	Al_2O_3	SiO_2	MnO	MnS	CuS	CuO	Al_2O_3	SiO_2	MnO	MnS	CuS	CuO
Inclusion	at%	at%	at%	at%	at%	at%	at%	at%	at%	at%	at%	wt%	wt%	wt%	wt%	wt%	wt%
1	26.32	39.82	4.89	22.77	6.2	27.06	49.12	18.73	0.00	4.02	1.08	36.74	39.30	17.69	0.00	5.12	1.14
2	26.88	34.98	9.01	25.02	4.11	27.98	43.69	20.83	4.08	3.42	0.00	41.01	37.74	21.25	4.65	4.28	0.00
3	23.38	40.15	5.83	22.42	8.21	24.34	50.15	18.67	0.00	4.86	1.98	36.39	44.19	19.42	0.00	6.24	2.12
4	27.61	39.16	1.4	26.96	4.86	27.59	46.96	21.56	0.00	1.12	2.77	39.27	39.38	21.34	0.00	1.43	2.94
5	32.44	42.88	0.3	20.75	3.63	31.37	49.76	16.05	0.00	0.23	2.58	43.65	40.80	15.54	0.00	0.29	2.71
6	38.47	39.25	0.43	18.17	3.68	37.33	45.71	14.11	0.00	0.33	2.52	50.39	36.36	13.25	0.00	0.41	2.58
7	35.63	33.36	1.29	24.55	5.18	35.83	40.26	19.75	0.00	1.04	3.13	48.89	32.37	18.75	0.00	1.27	3.18
8	34.02	36.87	3.48	22.96	2.65	34.22	44.50	18.48	0.67	2.13	0.00	46.69	35.78	17.54	0.75	2.64	0.00
9	27.15	42.57	1.54	28.13	0.61	26.63	50.10	22.07	0.73	0.48	0.00	37.24	41.29	21.48	0.86	0.62	0.00
10	35.3	34.46	0.39	26.1	3.76	35.11	41.13	20.77	0.00	0.31	2.68	47.58	32.84	19.58	0.00	0.38	2.75
11	26.3	40.94	0.52	29.56	2.68	25.98	48.54	23.36	0.00	0.41	1.71	36.68	40.37	22.95	0.00	0.53	1.84
12	33.29	36.73	1.06	23.42	5.5	33.12	43.86	18.64	0.00	0.84	3.53	46.05	35.92	18.03	0.00	1.05	3.65
13	30.22	37.97	1.3	27.16	3.35	30.16	45.48	21.69	0.00	1.04	1.64	41.86	37.19	20.94	0.00	1.31	1.72
14	33.24	38.97	0.61	25.16	2.01	32.67	45.96	19.78	0.00	0.48	1.10	44.44	36.84	18.72	0.00	0.60	1.15
15	29	36.13	0.7	30.55	3.62	29.09	43.49	24.52	0.00	0.56	2.34	40.53	35.70	23.77	0.00	0.71	2.47
16	32.07	39.15	2.37	25.41	0.99	31.67	46.39	20.07	1.09	0.78	0.00	43.40	37.46	19.14	1.25	0.98	0.00
17	32.46	40.78	0.24	24.04	2.49	31.63	47.69	18.74	0.00	0.19	1.75	43.47	38.61	17.92	0.00	0.24	1.84
18	38.16	38.32	2.43	20.31	0.78	37.29	44.93	15.88	1.29	0.61	0.00	49.84	35.39	14.77	1.44	0.75	0.00
19	31.96	40.02	0.81	27.14	0	31.23	46.92	21.21	0.63	0.00	0.00	42.41	37.55	20.04	0.73	0.00	0.00
20	30.27	42.12	0.48	25.93	1.2	29.53	49.30	20.23	0.00	0.37	0.56	40.64	39.98	19.38	0.00	0.48	0.60
Average	31.21	38.73	1.95	24.83	.28	31.03	46.21	19.74	0.42	1.14	1.47	43.10	37.82	19.08	0.48	1.43	1.54

Table 4-9. Chemical analysis of twenty inclusions and conversions into oxides for sample C2.12.

Sample C.2.13						Inclusion Compound Composition at%						Inclusion Compound Composition wt%					
	Al Ka	Si Ka	S Ka	Mn Ka	Cu Ka	Al_2O_3	SiO_2	MnO	MnS	CuS	CuO	Al_2O_3	SiO_2	MnO	MnS	CuS	CuO
Inclusion	at%	At%	at%	at%	at%	at%	at%	at%	at%	at%	at%	wt%	wt%	wt%	wt%	wt%	wt%
1	48.48	25.66	3.9	18.85	3.12	49.74	31.59	15.47	0.64	2.56	0.00	60.61	22.68	13.12	0.67	2.93	0.00
2	51.91	26.09	2.64	16.62	2.75	52.59	31.72	13.47	0.00	2.14	0.09	65.21	23.17	11.62	0.00	2.43	0.08
3	49.62	28.96	4.03	14.2	3.19	50.14	35.12	11.48	0.68	2.58	0.00	63.61	26.25	10.13	0.71	2.96	0.00
4	48.11	25.71	4.17	18.78	3.23	49.43	31.70	15.44	0.77	2.66	0.00	62.69	23.69	13.62	0.80	3.04	0.00
5	54.06	24	2.62	16.22	3.09	54.99	29.30	13.20	0.00	2.13	0.38	67.53	21.20	11.28	0.00	2.39	0.36
6	51.52	24.63	3.04	16.69	4.12	52.72	30.24	13.66	0.00	2.49	0.88	65.86	22.26	11.88	0.00	2.81	0.83
7	54.08	24.69	1.41	16.82	3	54.32	29.76	13.51	0.00	1.13	1.28	66.85	21.58	11.57	0.00	1.28	1.20
8	51.44	26.47	2.53	14.96	4.6	52.04	32.13	12.11	0.00	2.05	1.68	65.54	23.85	10.61	0.00	2.32	1.58
9	45.69	26.57	5.56	15.26	6.91	47.94	33.45	12.81	0.00	4.67	1.13	62.61	25.75	11.64	0.00	5.35	1.08
10	49.34	26.44	5.66	13.03	5.53	51.39	33.04	10.86	0.11	4.61	0.00	65.53	24.83	9.63	0.11	5.22	0.00
11	57.9	19.3	1.52	19.52	1.76	59.03	23.61	15.92	0.00	1.24	0.20	70.26	16.56	13.18	0.00	1.36	0.18
12	38.74	20.6	4.57	25.75	10.34	41.96	26.77	22.31	0.00	3.96	5.00	57.27	21.54	21.19	0.00	4.59	4.82
13	51.98	24.11	2.58	18.83	2.51	53.02	29.51	15.37	0.06	2.05	0.00	65.38	21.44	13.18	0.06	2.31	0.00
14	50.85	24.11	1.89	20.17	2.98	51.73	29.43	16.41	0.00	1.54	0.89	64.27	21.55	14.19	0.00	1.75	0.84
15	50	23.76	3.07	18.2	4.96	51.53	29.38	15.00	0.00	2.53	1.56	64.99	21.84	13.17	0.00	2.86	1.47
16	39.34	21.91	14.13	15.33	9.29	44.10	29.48	13.75	4.34	8.33	0.00	62.08	24.45	13.47	4.49	9.46	0.00
17	52.5	25.05	2.86	16.84	2.75	53.40	30.57	13.70	0.09	2.24	0.00	65.97	22.26	11.78	0.09	2.52	0.00
18	48.18	26.92	5.63	13.95	5.32	50.11	33.60	11.61	0.26	4.43	0.00	64.26	25.39	10.36	0.27	5.04	0.00
19	47.86	26.81	6.13	13.82	5.38	49.86	33.52	11.52	0.63	4.48	0.00	64.23	25.44	10.32	0.65	5.11	0.00
20	46.87	26.85	5.8	14.31	6.17	49.09	33.75	11.99	0.00	4.86	0.31	63.49	25.72	10.79	0.00	5.55	0.29
Average	**49.42**	**24.93**	**4.19**	**16.91**	**4.55**	**51.03**	**30.89**	**13.96**	**0.36**	**3.10**	**0.66**	**64.64**	**23.06**	**12.31**	**0.37**	**3.51**	**0.62**

Table 4-10. Chemical analysis of twenty inclusions and conversions into oxides for sample C2.13.

	Sample C.2.14					Inclusion Compound Composition at%						Inclusion Compound Composition wt%					
	Al Ka	Si Ka	S Ka	Mn Ka	Cu Ka	Al_2O_3	SiO_2	MnO	MnS	CuS	CuO	Al_2O_3	SiO_2	MnO	MnS	CuS	CuO
Inclusion	at%	at%	at%	at%	at%	at%	at%	at%	at%	at%	at%	wt%	wt%	wt%	wt%	wt%	wt%
1	75.55	12.15	2.8	7.56	1.95	76.76	14.81	6.15	0.69	1.59	0.00	83.58	9.50	4.66	0.64	1.62	0.00
2	81.83	8.71	2.1	6.77	0.58	82.34	10.52	5.45	1.22	0.47	0.00	89.18	6.71	4.11	1.11	0.47	0.00
3	80.1	10.59	2.86	4.2	2.24	81.36	12.91	3.41	0.50	1.82	0.00	89.07	8.33	2.60	0.46	1.83	0.00
4	64.62	12.97	10.22	5.7	6.5	69.54	16.75	4.91	3.20	5.60	0.00	83.96	11.92	4.12	3.01	5.78	0.00
5	80.76	9.45	2.88	5.29	1.62	81.88	11.50	4.29	1.02	1.31	0.00	89.35	7.39	3.26	0.93	1.31	0.00
6	79.1	14.35	0.67	4.65	1.24	78.29	17.04	3.68	0.00	0.53	0.45	86.13	11.05	2.82	0.00	0.54	0.38
7	70.82	13.58	4.38	5.07	6.15	73.70	16.96	4.22	0.00	3.65	1.47	85.07	11.54	3.39	0.00	3.75	1.26
8	75.63	7.84	0.15	12.03	4.35	77.06	9.59	9.81	0.00	0.12	3.42	86.07	6.31	7.62	0.00	0.12	2.89
9	65.69	4.18	8.21	6.94	14.98	74.44	5.68	6.29	0.00	7.44	6.14	90.60	4.08	5.33	0.00	7.43	5.10
10	58.98	20.63	0.75	18.25	1.39	59.31	24.89	14.68	0.00	0.60	0.51	70.44	17.42	12.13	0.00	0.66	0.47
11	67.28	12.79	0.83	14.74	4.36	68.72	15.68	12.04	0.00	0.68	2.88	79.59	10.70	9.71	0.00	0.71	2.52
12	69.38	12.52	3.83	12.08	2.19	71.43	15.47	9.95	1.35	1.80	0.00	81.67	10.42	7.91	1.28	1.87	0.00
13	63.46	14.78	4.6	13.97	3.19	66.07	18.46	11.64	1.17	2.66	0.00	77.69	12.79	9.52	1.13	2.81	0.00
14	75.67	10.71	3.17	8.07	2.38	77.60	13.18	6.62	0.65	1.95	0.00	86.25	8.63	5.12	0.60	1.98	0.00
15	60.87	12.52	8.83	6.73	11.04	67.55	16.67	5.97	0.00	7.84	1.96	82.85	12.05	5.10	0.00	8.13	1.69
16	77.98	9.04	2.35	5.51	5.12	80.12	11.15	4.53	0.00	1.93	2.28	89.18	7.31	3.51	0.00	1.94	1.90
17	80.43	7.06	1.69	8.87	1.95	82.44	8.68	7.27	0.00	1.39	0.21	89.01	5.52	5.46	0.00	1.38	0.18
18	73.59	10.48	3.24	8.86	3.83	76.40	13.06	7.36	0.00	2.69	0.49	85.64	8.62	5.74	0.00	2.74	0.42
19	72.87	8.38	5.56	7.32	5.88	77.95	10.76	6.26	0.00	4.76	0.27	87.93	7.15	4.92	0.00	4.78	0.23
20	72.74	20.99	0.58	4.2	1.49	70.98	24.58	3.28	0.00	0.45	0.71	80.89	16.51	2.60	0.00	0.48	0.62
Average	72.37	11.69	3.49	8.34	4.12	74.73	14.48	6.89	0.49	2.39	1.01	84.87	9.69	5.44	0.45	2.45	0.86

Table 4-11. Chemical analysis of twenty inclusions and conversions into oxides for sample C2.14.

	Sample C.2.15					Inclusion Compound Composition at%						Inclusion Compound Composition wt%					
	Al Ka	Si Ka	S Ka	Mn Ka	Cu Ka	Al_2O_3	SiO_2	MnO	MnS	CuS	CuO	Al_2O_3	SiO_2	MnO	MnS	CuS	CuO
Inclusion	at%	at%	at%	at%	at%	at%	at%	at%	at%	at%	at%	wt%	wt%	wt%	wt%	wt%	wt%
1	95.195	2.17	0	0.511	2.122	95.29	2.61	0.41	0.00	0.00	1.70	96.80	1.56	0.29	0.00	0.00	1.35
2	97.011	2.988	0	0	0	96.44	3.56	0.00	0.00	0.00	0.00	97.87	2.13	0.00	0.00	0.00	0.00
3	93.547	2.268	0	0	4.183	93.91	2.73	0.00	0.00	0.00	3.36	98.31	1.69	0.00	0.00	0.00	2.67
4	89.139	4.95	0	0.308	5.601	89.31	5.95	0.25	0.00	0.00	4.49	96.04	3.77	0.18	0.00	0.00	3.63
5	91.044	3.088	0.427	0.497	4.941	91.87	3.74	0.40	0.00	0.34	3.64	97.37	2.34	0.30	0.00	0.33	2.92
Average	**93.19**	**3.09**	**0.09**	**0.26**	**3.37**	**93.37**	**3.72**	**0.21**	**0.00**	**0.07**	**2.63**	**97.56**	**2.29**	**0.15**	**0.00**	**0.07**	**2.10**

Table 4-12. Chemical analysis of twenty inclusions and conversions into oxides for sample C2.15.

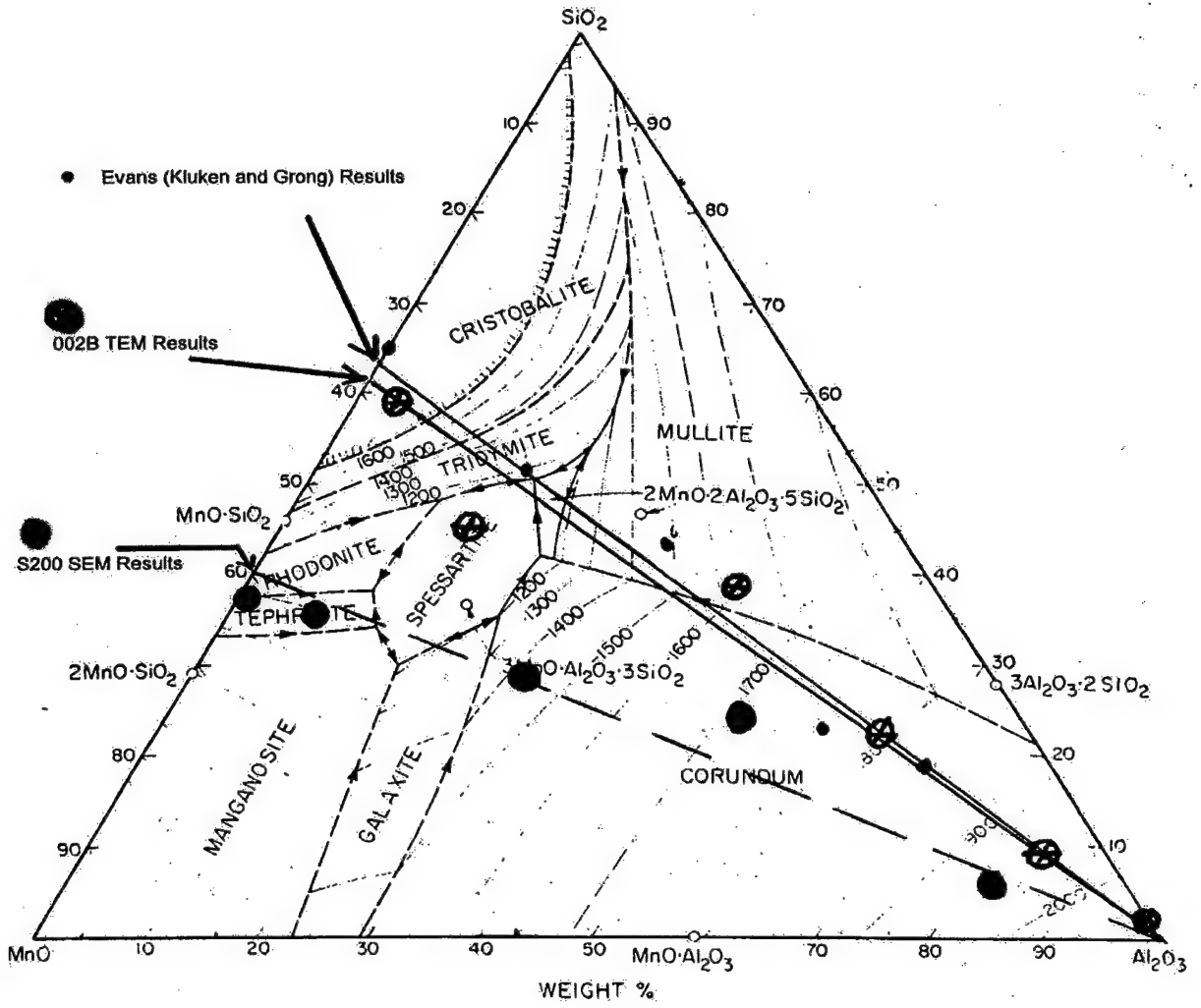

Figure 4-11. Ternary diagram with current and previous work chemical composition.

2. Morphology and Diffraction Patterns

To understand the possible mechanisms of acicular ferrite nucleation, especially when low amounts are being nucleated as in the present work, crystal structures and micrographs through diffraction patterns and scanning transmission electron microscopy imaging are useful. As the chemical analysis was being performed, the inclusion shape was observed for all the samples. For samples C2.10 through C2.12, the inclusions looked spherical with no facets. A typical STEM image for C2.11 with its spectrum is shown in Fig. 4-12. It can be seen that the non-metallic inclusion is quite spherical. For samples C2.13 through C2.15, nearly all inclusions show facets, and these are believed to help acicular ferrite to nucleate. A STEM image for sample C2.15 with its spectrum is shown in Figure 4-13. This inclusion clearly shows a facet as labeled in the figure. The facetted edges are typical in inclusions that promote acicular ferrite nucleation. The nickel peak in the spectra is caused by the nickel grid on which the carbon extractions were placed.

Diffraction patterns were examined for all inclusions studied. For the C2.10 sample, a diffraction pattern was observed from the oxide region and appeared to be a non-cubic crystal structure, probably triclinic. This correlates well with cristobalite or rhodonite ($MnO.SiO_2$), both of which have triclinic crystal structures. The chemical composition of the oxides in the inclusions are indicated on the ternary diagram in Figure 4-10. For samples C2.11 and C2.12, only amorphous ring diffraction patterns were observed from the oxide components. This implies that the inclusions were amorphous due to low melting points and rapid cooling rates in welding. The chemical composition for the inclusions in sample C2.11 places them in the spessartite region, and the

composition of inclusions of sample C2.12 appears to be in the mullite region. Amorphous inclusions obviously cannot nucleate acicular ferrite by epitaxy since they have no crystal structure and indeed, we found that the inclusions only nucleate small amounts (~10-12%) of acicular ferrite. However, for samples C2.13 through C2.15, the diffraction patterns were found to be consistent with corundum. Since the corundum inclusions have a cubic crystal structure, it seems that the acicular ferrite may form by lattice matching on these inclusions. This has in fact been observed by Grong et al. [Ref.15], who have demonstrated convincingly that γ-Al_2O_3 nucleates acicular ferrite by epitaxy. The results of the present work also clearly support the theory of acicular ferrite nucleation by epitaxy for these alumina inclusions. In the work of Mahoney [Ref. 37] and Blais et al. [Ref. 26] where inclusions containing large amounts of titanium oxide were generated, Figures 4-1 through 4-3 clearly show that much greater amounts of acicular ferrite are generated than in the present work. This suggests perhaps that titanium-containing oxide inclusions are far more effective at nucleating acicular ferrite by some other mechanism other than epitaxy. This is possibly a chemical reaction, similar to those discussed by Gregg et al. [Ref. 32].

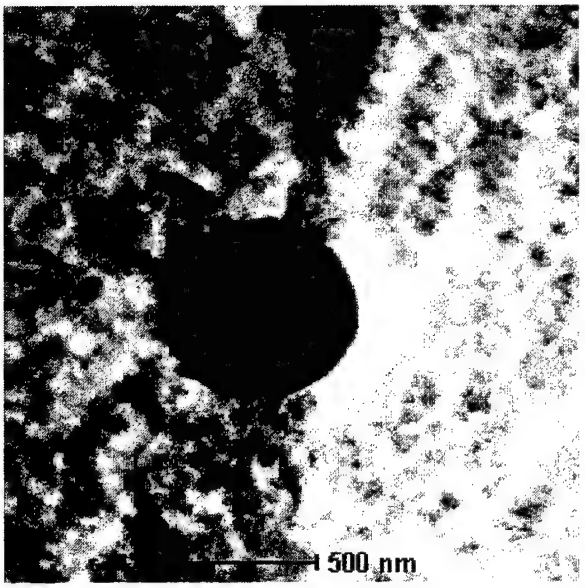

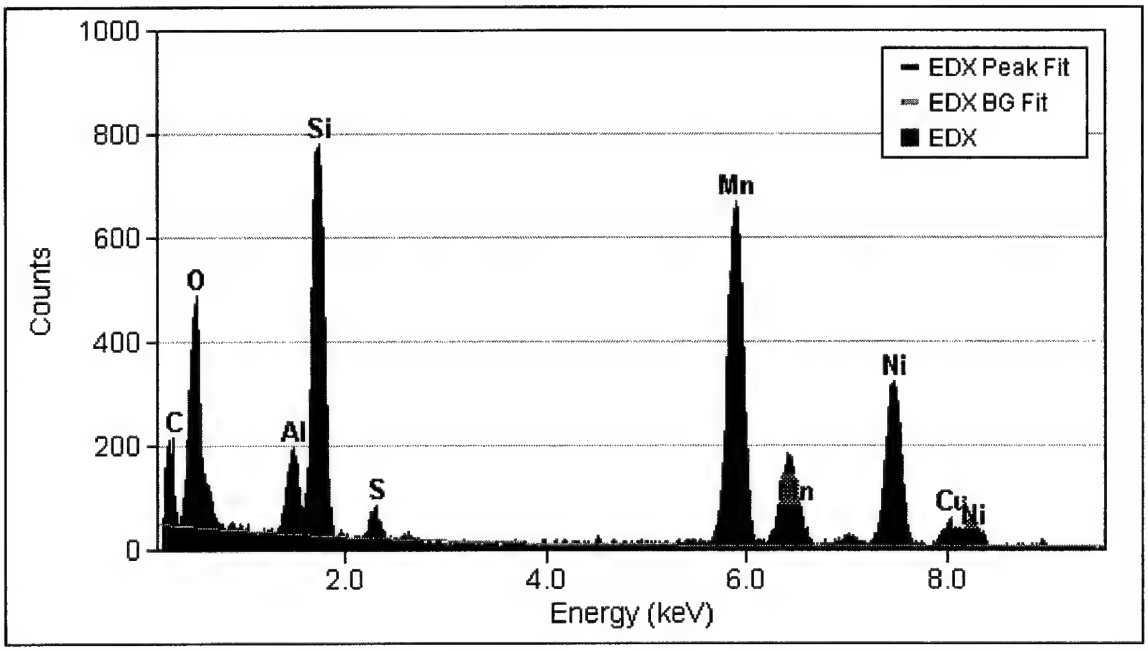

Figure 4-12. STEM image of an inclusion and its EDX spectra for sample C2.11.

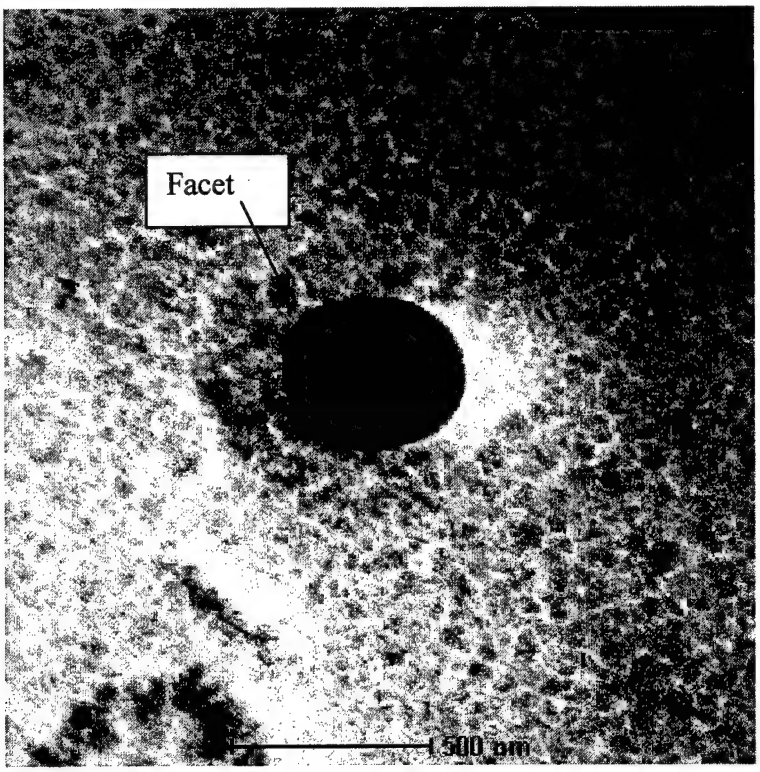

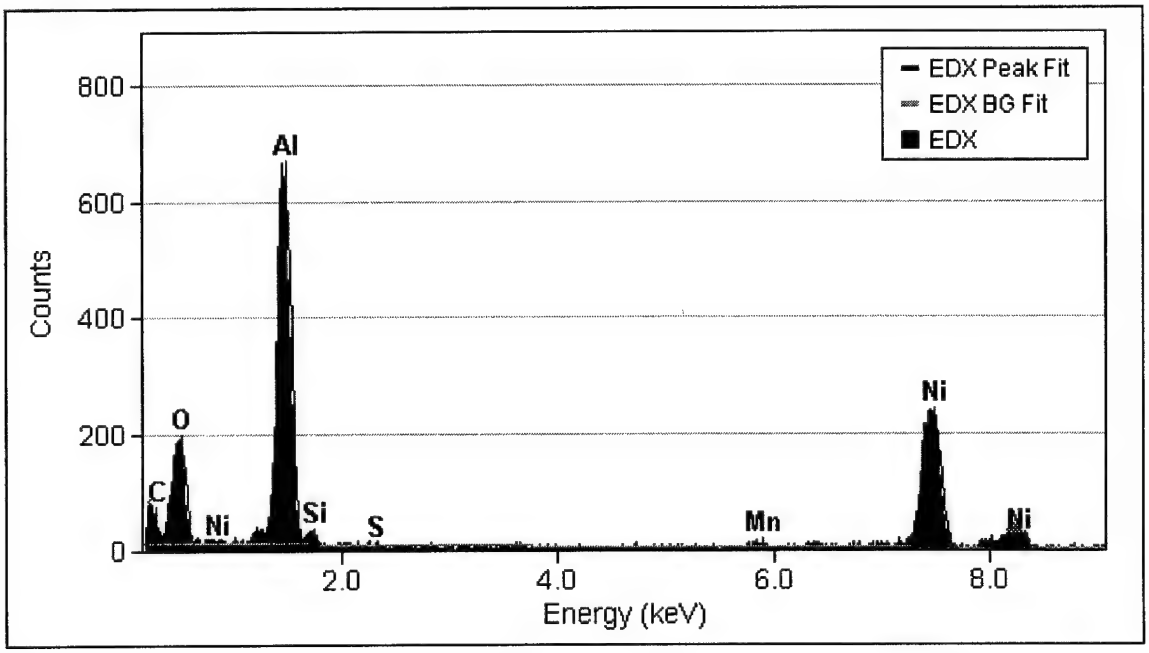

Figure 4-13. STEM image of an inclusion and its EDX spectra for sample C2.15.

THIS PAGE INTENTIONALLY LEFT BLANK

V. SUMMARY

A. CONCLUSIONS

The strength and toughness of weld metal in C-Mn steels is increased by additions of aluminum to the weld metal. These are two reasons for this. The first is that the inclusions are small and there are less of them to act as microvoid initiation sites. The second is that more acicular ferrite nucleates as the weld metal aluminum content is increased and this improves the weld metal toughness.

The average size of the inclusions ranged from 0.52 - 0.57 μm. These sizes can almost be considered the same within experimental error. Higher aluminum contents promote the nucleation of acicular ferrite so that heterogeneous nucleation does not appear to be the only nucleation mechanism for the samples studied in the present work.

For sample C2.10, the mechanism by which the inclusions nucleate acicular ferrite is heterogeneous nucleation plus strain energy (if present). The crystal structure is non-cubic so lattice matching does not appear possible.

The mechanism by which the inclusions for samples C2.11 and C2.12 nucleate acicular ferrite also appears to be heterogeneous nucleation and possibly strain energy. The glassy diffraction patterns were clearly visible so epitaxy cannot be a mechanism of acicular ferrite nucleation in these samples.

For samples C2.13 through C2.15, the chemical composition and diffraction patterns of the inclusions indicate that they have the γ-Al_2O_3 cubic crystal structure (distorted spinel). This has been shown to have good lattice matching with ferrite so that acicular ferrite can be nucleated by epitaxy for these.

It does seem, then, that the mechanism of epitaxy does promote acicular ferrite nucleation, but the effectiveness is possibly less than that associated with the chemical reactions at the inclusion/austenite interfaces associated with titanium oxides. The effectiveness of the four mechanisms associated with the nucleation of acicular ferrite can be listed from strongest to weakest. They are: chemical effects at the inclusion/austenite interface, epitaxy, strain energy, and heterogeneous nucleation. The latter two mechanisms always operate irrespective of inclusion chemistry or crystallography.

B. SUGGESTIONS FOR FURTHER RESEARCH

A more thorough TEM investigation of the inclusion/matrix interface needs to be conducted to actually determine if epitaxy exists in the samples studied in the present work.

Instead of carbon extraction replicas, thin foils of the weld metal samples should be investigated to determine if lattice matching between the ferrite and γ-Al_2O_3 agrees with the previous work of Kluken and Grong

Inclusion samples should be analyzed using EDX and PEELS mapping to further refine the chemical composition of the inclusion.

Other welding techniques should be used to provide samples with similar overall chemical composition in order to investigate whether the conclusions of the present work can be applied to weld metals generated by other arc welding processes.

LISTS OF REFRENCES

1. Kou, S., *Welding Metallurgy*, John Wiley and Sons, New York, 1987.

2. Harrison , P. L. and Farrar, R. A., "Influence of Oxygen-Rich Inclusions on the Austenite-to-Ferrite Phase Transformations in High-Strength-Low-Alloy (HSLA) Steel Weld Metals," *Journal of Materials Science*, 16:2218-2226, 1981.

3. *Guidelines for Classification of Ferritic Steel Weld Metal Microstructural Constituents using the Light Microscope*. IIW Doc. No. IXJ-102-85.

4. Bhadeshia, H.K.D.H., "Control of Weld Metal Microstructure and Properties," *The Metallurgy, Welding, and Qualification of Microalloyed (HSLA) Steel Weldments*, American Welding Society, 1990.

5. Bhadeshia, H.K.D.H., *Bainite in Steels*, The Institute of Materials, London, Chapter 10, 1990.

6. Strangwood, M. and Bhadeshia, H.K.D.H., "The Mechanism of Acicular Ferrite Formation in Steel Weld Deposits," *Advances in Welding Science and Technology*, ASM, Metals Park, Ohio, 1987.

7. Yang, J.R. and Bhadeshia, H.K.D.H., "Orientation Relationship Between Adjacent Plates of Acicular Ferrite in Steel Weld Deposits," *International Conference on trends in Welding Research*, ASM International, 1989.

8. Ricks, R.A., Howell, P.R., and Barrite, G.S., "The Nature of Acicular Ferrite in HSLA Steel Weld Metals," *Journal of Materials Science*, 1982.

9. Reed, R.C. and Bhadeshia, H.K.D.H., "A Simple Model for Multi Pass Steel Welds," *Acta Metall. Mater.*, Vol. 42, No. 11, pp. 3663-3678, 1994.

10. *Metals Handbook Ninth Edition, Volume 6 Welding, Brazing, Soldering*, American Society of Metals. Metals Park, Ohio, 1983.

11. Kiessling, R.K., *Non-metallic Inclusions in Steel, Part V*, The Institute of Metals, 1989.

12. Babu, S.S., David, S.A., Vitek, J.M., Mundra, K.,and Debroy, T., "Development of Macro- and Microstructures of C-Mn Low Alloy Steel Welds: Inclusion Formation," *Materials Science and Technology 11*, 1995.

13. Bhatti, A.R., Sagesse, M.E., Hawkins, D.N., Whiteman, J.A., and Golding, M.S., "Analysis of Inclusions in Submerged Arc Welds in Microalloyed Steels," *Welding Research Supplement*, 1984.

14. Evans, G.M., "The Effect of Aluminum in Shielded Metal Arc C-Mn Steel Multipass Deposits," *Welding research Supplement*, 1991.

15. Grong, O., Kluken, A.O., Nylund, H.K., Dons, A.L., Hjelen, J., "Catalyst Effects in Heterogeneous Nucleation of Acicular Ferrite," *Metallurgical and Materials Transactions A*, Volume 26A, March 1995.

16. Kluken, A.O., Grong, O., Rorvik, G., *Metallurgical Transactions A*, 21A:2047-2058, July 1990.

17. Kiessling, R. and Lange, N., "Non-Metallic Inclusions in Steel," *The Metal Society*, 1978.

18. Fox, A.G., Eakes, M.W., and Franke, G.L., "The Effect of Small Changes in Flux Basicity on the Acicular Ferrite Content and Mechanical Properties of Submerged Arc Weld Metal of Navy HY-100 Steel," *Welding Research Supplement*, October 1996.

19. Fox, A.G. and Brothers, D.G., "The Role of Titanium in the Non-Metallic Inclusions Which Nucleate Acicular Ferrite in the Submerged Arc Weld (SAW) Fusion Zones of Navy HY-100 Steel," *Scripta Metallurgica et Materiala*, 1995.

20. Komizo, Y. and Fukada, Y., "Toughness Improvement in Weld Metal of Carbon and HSLA Steels in Japan," Sumitomo Metals Industries, Ltd., 1986.

21. Abson, D.J. and Pargeter, R.J., "Factors Influencing As-deposited Strength, Microstructure, and Toughness of Manual Metal Arc Welds Suitable for C-Mn Steel Fabrications, *International Metals Review*, Volume 31, No. 4, 1986.

22. Walters, J., "Microchemical Analysis of Non-Metallic Inclusions in C-Mn Steel Shielded Metal Arc Welds by Analytical Transmission Electron Microscopy," Master's Thesis. Naval Postgraduate School, 1998.

23. Greene, M.K., "The Effects of Titanium on the Mechanical Properties of Shielded Metal Arc Welding (SMAW) of C-Mn Steels," Master's Thesis, Naval Postgraduate School, 1997.

24. Yamamoto, K., Matsuda, S., Haze, T., Chijiiwa, R., and Mimura, H., *Proceedings of a Conference on Residual and Unspecified Elements in Steels*, ASM International, 1987.

25. Abson, D.J., "Nonmetallic Inclusions in Ferritic Steel Weld Metals," *International Institute for Welding*, Document IX-1486-87, 1987.

26. Blais, C., L'Esperance, G., and Evans, G.M., "Characterisation of Inclusions Found in C-Mn Steel Welds Containing Titanium," *Science and Technology of Welding and Joining*, Volume 4, No. 3, pp. 143-150, 1999.

27. Muan, A. and Osborn, E.F., *Phase Equilibrium Among Oxides in Steelmaking*, Addison-Wesley Publishing Company, 1965.

28. Zhang, Z. and Farrar, R.A., "Role of Non-Metallic Inclusions in Formation of Acicular Ferrite in Low Alloy Weld Metals," *Materials Science and Technology*, Volume 12, 1996.

29. Babu, S.S. and Bhadeshia, H.K.D.H., "Mechanism of the Transition from Bainite to Acicular Ferrite." *Materials Transactions*, JIM, 32, 679,1991.

30. Brooksbank, D. and Andrews, K.W., "Stress Fields Around Inclusions and Their Relation to Mechanical Properties," *Journal of the Iron and Steel Institute*, 210:246-255. 1972.

31. Babu, S.S. and Bhadeshia, H.K.D.H, "Stress and the Acicular Ferrite Transformation," *Materials Science and Engineering*, A156, pp. 1-9, 1992.

32. Gregg, J.M. and Bhadeshia, H.K.D.H, "Solid-State Nucleation of Acicular Ferrite on Minerals Added to Molten Steel," *Acta Materiala*, Volume 45, No. 2, pp. 739-748, 1997.

33. Mizuno, M., Tanaka, I., and Adachi, H. "Chemical Bonding at the Fe/TiX (X=C, N or O) Interfaces," *Acta Materiala*, Volume 46, No. 5, pp. 1637-1645, 1998.

34. Dowling, J.M., Corbett, J.M. and Kerr, H.W., "Inclusion Phases and the Nucleation of Acicular Ferrite in Submerged Arc Welds in High Strength Low Alloy Steels," *Metallurgical Transactions A*, 1986.

35. Evans, G.M. and Bailey, N., *Metallurgy of Basic Weld Metal*, Abington Publishing, Woodhead Publishing Ltd., Cambridge, England, 1997.

36. Fullman, R.L., *Measurement of Particle Size in Opaque Bodies*, TRANS AIME, 197, p. 447, 1953.

37. Mahoney, M.F., "Investigation into the Mechanism of Acicular Ferrite Nucleation in Steel Weld Metal," Master's Thesis, Naval Postgraduate School, 1999.

38. Kluken, A.O. and Grong, O., "Mechanisms of Inclusion Formation in Al-Ti-Si-Mn Deoxidised Steel Weld Metals," *Metall. Trans A*, Vol. 20A, pp. 1335-49, 1989.

39. Franklin, A.G., *J. Iron Steel Inst.*, 207, pp. 181-186, 1969.

THIS PAGE INTENIONALLY LEFT BLANK

INITIAL DISTRIBUTION LIST

1. Defense Technical Information Center 2
   8725 John J. Kingman Road, Suite 0944
   Ft. Belvoir, VA 22060-6218

2. Dudley Knox Library 2
   Naval Postgraduate School
   411 Dyer Road
   Monterey, CA 93943-5100

3. Naval/Mechanical Engineering, Code 34 1
   Naval Postgraduate School
   700 Dyer Road, Bldg. 245
   Monterey, CA 93943-5100

4. Department Chairman, Code ME/Mc 1
   Department of Mechanical Engineering
   Naval Postgraduate School
   700 Dyer Road, Bldg. 245
   Monterey, CA 93943-5100

5. Dr. Alan G. Fox, Code ME/Fx 2
   Department of Mechanical Engineering
   Naval Postgraduate School
   700 Dyer Road, Bldg. 245
   Monterey, CA 93943-5100

6. Mr. Joe Blackburn 1
   Naval Surface Warfare Center
   Carderock Division, Code 615
   9500 McAurthur Boulevard
   Bethesda, Maryland 20084-5000

7. Dr. G. M. Evans 1
   2 Seabank Court
   178 Banks Road
   West Kirby, Wirral CH48 ORH United Kingdom

8. LT Craig A. Hackstaff..... 2
1529 Ulster Way
West Chester, Pa. 19380

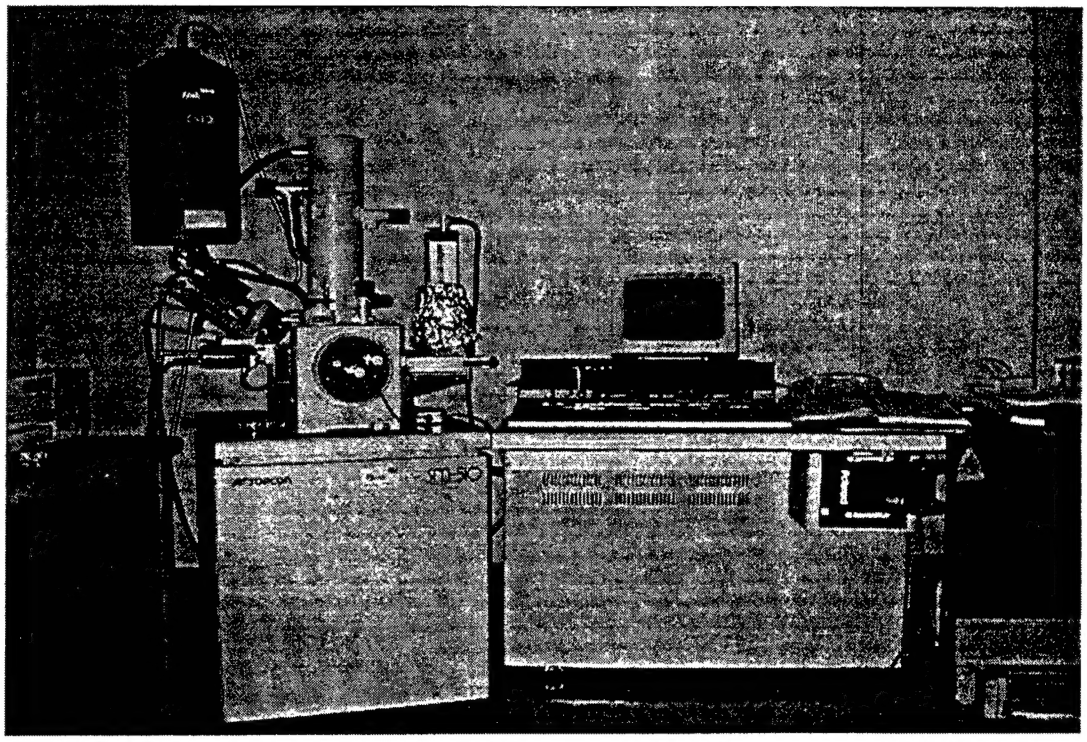

(a)

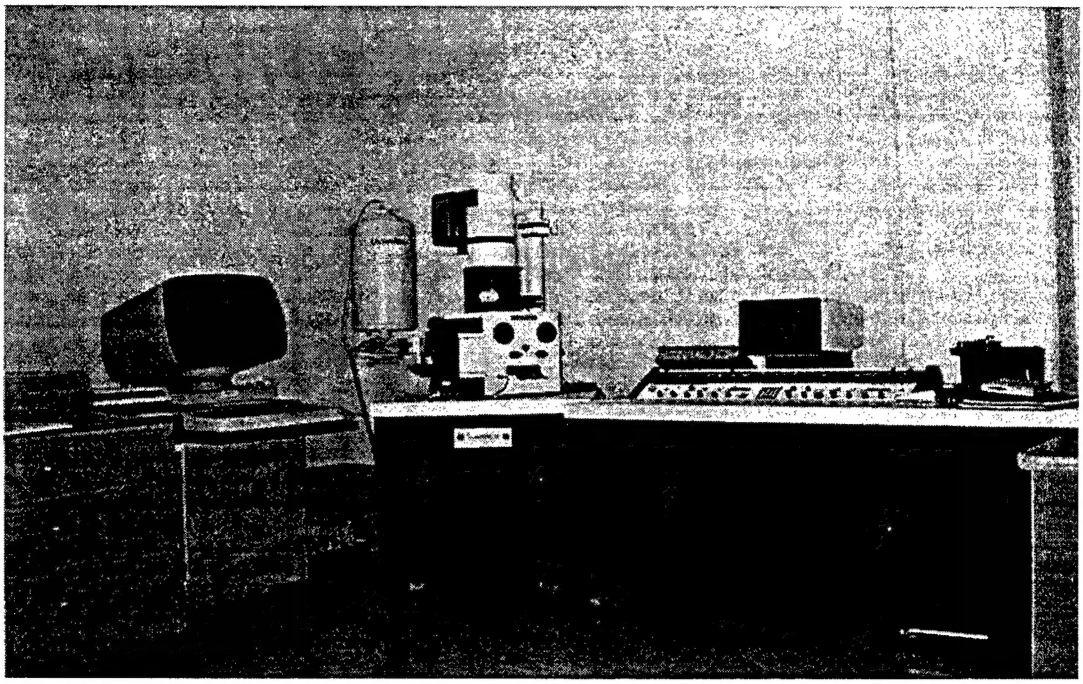

(b)

Figure 3-1. The Topcon SM 510 (a) and Cambridge S200 (b) SEMs at the Naval Postgraduate School.